Aalto University
School of Chemical
Technology

School of Chemical Technology
Degree Programme of Chemical Technology

José Valentín Gómez Fuentes

SIMULATION ENVIRONMENT FOR ADVANCED CONTROL DEVELOPMENT OF A MULTIPLE HEARTH FURNACE

Master's thesis for the degree of Master of Science in Technology submitted for inspection, Espoo, 25.04.2016.

Supervisor Professor Sirkka-Liisa Jämsä-Jounela

Instructor Ph.D. Alexey Zakharov

Aalto University
School of Chemical
Technology

Aalto University, P.O. BOX 11000, 00076
AALTO
www.aalto.fi

Abstract of master's thesis

Author	José Valentín Gómez Fuentes
Title of thesis	Simulation Environment for Advanced Control Development of a Multiple Hearth Furnace
Department	Department of Biotechnology and Chemical Technology
Professorship	Process control
Code of professorship	Kem-90
Thesis supervisor	Professor Sirkka-Liisa Jämsä-Jounela
Thesis advisor(s) / Thesis examiner(s)	Ph.D. Alexey Zakharov
Date	31.03.2016
Number of pages	95
Language	English

Abstract

The aim of this thesis is to setup a simulation environment that prepares the ground for Multiple Hearth Furnace (MHF) advanced process control development based on Economic Model Predictive Control (EMPC) and/or MPC techniques.

Additionally, the interest is to design an Economic MPC for the Multiple Hearth Furnace, aiming to minimize energy consumption of the furnace while maintaining the specified product quality. The implementation of the EMPC requires a dynamic model which is simplified from a previously developed mechanistic model of the MHF. The simplified model is developed in the form of a nonlinear Hammerstein-Wiener model, which is linearized at every sampling time to carry out the state estimation and MPC optimization tasks. As the accuracy of the simplified process model is crucial for performance of the EMPC, the thesis aims to compare the simulation results of the mechanistic model and the simplified one. The comparison of the models show that the simplified model follows accurately the mechanistic model in all cases.

A description of the process of interest is given, with an emphasis in outlining the overall control strategy currently implemented. Next the components of the EMPC design are illustrated, including the overall strategy, the cost function and the necessary models of the process. Afterwards an implementation algorithm is provided comprising all the elements of the design, in order to obtain the optimal control of the MHF. Finally, practical problems regarding industrial implementations of temperature control in the hearth 4 are discussed and further research items outlined.

Keywords Economic MPC, MPC, kaolin, calcination, Multiple Hearth Furnace

Acknowledgements

This master's thesis has been written in the Research Group of Process Control and Automation, at Aalto University School of Chemical Technology during the period 17. August 2015 – 31. March 2016. This work is a part of the STOICISM project. STOICISM (The Sustainable Technologies for Calcined Industrial Minerals) is a major innovative research project which has been supported by the European Commission under the 7th Framework Programme through the grant number 310645, for the "New environmentally friendly approaches to mineral processing".

I would like to thank professor Sirkka-Liisa Jämsä-Jounela for the opportunity to write my master's thesis in the research group, and particularly in this project. Her guidance, and advice are appreciated. Also, I would like to thank my instructor, Ph.D. Alexey Zakharov, for his expertise and support during the course of the work. Gratitude to my coworkers Jukka, Miao, Palash, Sasha, Rinat for making a proper work environment where one could work peacefully.

I very much appreciate the help received from the personnel of IMERYS in this work.

Sincerely, I would like to express my gratitude to my Family, to my parents and sisters, for their never-ending support and help through the years. To my brother in heaven who made me grow as a better man. To my friends, whom I value and keep close to my heart. To my colleagues and friends during the course of my studies, Moses, Igor, Anatoly, thank you for the good moments they will always be cherished.

"Aspiciens pro veritate"

Espoo 10.03.2016

José Valentín Gómez Fuentes

Table of Contents

Abbreviations

ARIMA	Auto Regressive Integrated Moving Average
BtoB	Burner-to-Burner
CARIMA	Controlled Auto Regressive Moving Average
CV	Controlled variables
DCS	Differential scanning calorimetry
DMC	Dynamic Matrix Control
DMPC	Distributed Model Predictive Control
EMPC	Economic model predictive control
HWM	Hammerstein-Wiener model
MHF	Multiple Hearth Furnace
MIMO	Multi input/multi output
MPC	Model Predictive Control
MV	Manipulated variables
PRBS	Pseudo-Random Binary Sequence
QP	Quadratic Program
RTO	Real Time Optimization

Notation

$\mathbb{I}_{\geq a}$	set of integer numbers greater than or equal to a $\in \mathbb{R}$
e_t	White noise
r_t	System setpoint(s) at sampling instant t
u_t	System input(s) at sampling instant t
x_t	System states(s) at sampling instant t
$\hat{x}(t+i\|t)$ $\hat{x}_{t+i}$	expected value of $x(t+i)$ with available information at instant t
y_t	System output(s) at sampling instant t
$\mathcal{K}$	A function $\alpha: \mathbb{R}_{\geq 0} \rightarrow \mathbb{R}_{\geq 0}$ is a class $\mathcal{K}$ function (or $\alpha \in \mathcal{K}$ for short), if it is continuous, strictly increasing, and $\alpha(0) = 0$
$\mathcal{K}_\infty$	A function $\alpha: \mathbb{R}_{\geq 0} \rightarrow \mathbb{R}_{\geq 0}$ is a class $\mathcal{K}_\infty$ function (or $\alpha \in \mathcal{K}_\infty$ for short), if $\alpha \in \mathcal{K}$ and $\alpha(\mathrm{r}) \rightarrow \infty$ for $\mathrm{r} \rightarrow \infty$
F_K	feed rate of kaolin
F_C	calcined kaolin
F_{g4}	Gas flow to Hearth 4
F_{g6}	Gas flow to Hearth 6
F_g	Total gas flow
p_c	Selling price of calcined kaolin
p_g	Price of methane gas
c_{H2O}	Water content
c_{fm}	Free moisture content

1 Introduction

Model Predictive Control (MPC) is a control strategy that has been implemented successfully in industry for more than 30 years and has attracted the interest of both the industrial and academic communities. Since its early development in 1978 [1], it has improved, in many ways, the manner that processes are controlled, specifically the prediction of process behavior [2].

Operational efficiency is an important aspect in chemical processes, but also economic goals are important. In recent years new improvements have been made to MPC so it may take into consideration the economic indicators as an objective function to optimize directly in real time the economic performance of the process [3]. This improvement is known as economic model predictive control (EMPC).

EMPC includes in its internal routines a general cost function, reflecting the economics of the process [4], as an objective function. Therefore, the process may be optimized economically in a dynamic time-variant approach. This approach presents an advantage compared to other methodologies that employ Real Time Optimization (RTO) to optimize the process in steady-state at a given specific time.

EMPC has been used in a number of industrial applications, including fermentation process [5], operation of gas pipes [6], oil sand primary separation vessel [7], Building Climate Control in a Smart Grid [8], and chemical process network [9]. Although this control strategy could also be applied to the mining industry, no studies have yet attempted to implement EMPC strategies in this industry. Traditionally, the mining industry has relied on single-loop PID controllers in grinding mill circuits [10]. By implementing EMPC more broadly in

the mining industry, the economic performance would improve, since this industry is driven by economic indicators and market prices of the minerals.

The aim of this thesis is to design a simulation environment for testing advanced control strategies in a Multiple Hearth Furnace used for kaolin calcination, as part of a kaolin processing chain. In order to accomplish this, an economic model predictive control strategy is developed for the simulation environment. The furnace considered in this work is a Herreschoff calciner, which is a large upright cylindrical furnace with eight different chambers, these chambers are commonly denominated as hearths.

The main two components of the simulation environment include the multiple hearth furnace model and an economic MPC strategy for controlling the furnace for minimizing its energy consumption while maintaining the specified product quality. Additionally, the current temperature control in Hearth 4 is analyzed in order to improve its performance in this part of the process.

LITERATURE PART

The literature part consists of introductory concepts on the model predictive control theory. Chapter 2 presents the fundamental concepts of MPC, including process modelling, the objective function, and the control law, which are necessary to understand this advanced control strategy. Furthermore, it reviews several MPC algorithm in Section 2.5, and discusses the MPC stability. Chapter 3 expands the previous concepts to incorporate process economics to the denominated Economic Model Predictive Control. Moreover, this Chapter provides basic properties and concepts on the control strategy of interest. Finally Chapter 4 provides an insight on calcination, including the physical and chemical phenomena that occurs within this process.

2 Fundamentals of Model Predictive control

This Chapter presents in Section 2.1 the model structure used in control theory. Section 2.2 shows prediction methods, Section 2.3 explains the necessary objective function and constraints and Section 2.4 describes the control law. Section 2.5 reviews a few commonly used MPC methods, while Section 2.6 provides the methods to ensure stability in MPC.

Model Predictive Control is an advanced process control strategy, using a model to foresee the future behavior of a process and to apply the proper corrective control actions leading the process to a desired state. In general, the objective of MPC is to drive the output variables to their selected setpoints, while preventing violations of the input and output constraints. In addition, MPC aims to avoid excessive movement of the input variables and to control as many process variables as possible even when a sensor or actuator is not available [11].

MPC algorithms may vary from each other but include the following common elements [12]: a prediction model, objective function and algorithms to obtain the control law. Choosing different options for these elements, allows different MPC implementations to be obtained.

2.1 Process and Disturbance Models

The key element of MPC is a process model, which states the relationship between the input and the output of a physical plant or a process. A disturbance model can be also used to develop a state estimator or to describe the plant model mismatch. Various MPC implementations, utilize many forms of process models [13], some of these are shown in this section.

2.1.1 Impulse response model

The impulse response model is defined as the convolution of the input sequence u_i and the impulse response f_i:

$$y_t = \sum_{i=1}^{\infty} f_i u_{t-i} \qquad (1)$$

where the impulse response f_i is the sampled output of the system stimulated by a unit impulse input. This sum is generally truncated where only values till N_S are considered, where N_S is the settling time of the process.

This models has the following advantages:

- Admits complex dynamics, such as delays, to be described with ease.
- Reflects, in an intuitive and clear way, the effect of each manipulated variable.

The model has two disadvantages:

- Is necessary to have a significant number of parameters
- May only be represented by stable processes without integrators

2.1.2 Step response model

The step response model is defined as follows:

$$y_t = \sum_{i=1}^{\infty} g_i \Delta u_{t-i} \quad (2)$$

Where $\Delta u_t = u_t - u_{t-1}$ and g_i is the sampled output of the system disturbed by the unitary step input. In stable systems, the step response g_i is a constant after the settling time N_S. The relation between the impulse and the step responses is as follows:

$$f_i = g_i - g_{i-1} \quad (3)$$

$$g_i = \sum_{j=1}^{i} f_j \quad (4)$$

Step response models present matching advantages and disadvantages, compared to the impulse response models.

2.1.3 Transfer function model

The transfer function model is defined in the Laplace or Z-transform domains. However, assuming z^{-1} acts as a time delay operator, the following notations are frequently used:

$$y_t = \frac{B(z^{-1})}{A(z^{-1})} u_t \quad (5)$$

The advantages of this model type include:

- Is suitable to describe unstable processes
- Requires fewer parameters.

The disadvantages are:

- The structure of the process is essential for identification, specifically the orders of A and B.
- Certain processes may not be described adequately by a low-order transfer function model.

2.1.4 State Space Model

A linear state-space is described by the following equations:

$$x_{t+1} = Ax_t + Bu_t \quad (6)$$

$$y_t = Cx_t + Du_t \quad (7)$$

The state-space models possess the following advantages:

- Multivariate processes are represented in the same way as SISO dynamics.
- Modern control theory and analysis methods, including a Kalman filter, may be applied with ease to state space models.

Disadvantages

- A few processes may not be described adequately by a state-space model with a limited number of states.

2.1.5 Time Series Model for the Disturbance

A widely used disturbance model is the Auto Regressive Integrated Moving Average (ARIMA), where the disturbance, representing the difference between the calculated output and measured output, is given by the following expression [14]:

$$d_t = \frac{C\left(z^{-1}\right)}{\Delta D\left(z^{-1}\right)} e_t \quad (8)$$

where d_t is the disturbance, e_t is the white noise, the symbol Δ denotes $1-z^{-1}$, and C and D are polynomials sometimes selected to be 1.

2.2 Multiple step ahead prediction

In MPC, the process model is used to design predictors of the future plant behavior, and subsequently the control law is devised utilizing the designed predictors. Based on multiple step ahead predictions, the future input actions of the process are selected to drive the process outputs towards the desired values. In the following equations (9)-(13), the multiple step ahead prediction is discussed in more details.

The simple model is considered, which is a slight modification of the conventional ARX model, including term Δu_t instead of u_t:

$$y_t = -ay_{t-1} + b\Delta u_{t-1} + e_t \tag{9}$$

The one-step ahead prediction is obtained by considering the model equation at time instant $t+1$

$$y_{t+1} = -ay_t + b\Delta u_t + e_{t+1} \tag{10}$$

If the white noise is ignored, then expressing the previous equation in prediction terms:

$$\hat{y}(t+1|t) = -ay_t + b\Delta u_t \tag{11}$$

In order to get a two-steps ahead prediction, the modeling equation is considered at the time instant $t+2$:

$$y_{t+2} = -ay_{t+1} + b\Delta u_{t+1} + e_{t+2} \tag{12}$$

Substituting equation *(10)* in equation *(12)*, then:

$$\begin{aligned} y_{t+2} &= -a(-ay_t + b\Delta u_t + e_{t+1}) + b\Delta u_{t+1} + e_{t+2} \\ &= a^2 y_t + b\Delta u_{t+1} - ab\Delta u_t - e_{t+1} + e_{t+2} \end{aligned} \tag{13}$$

The two-step ahead prediction is obtained by ignoring the unknown future noise values:

$$\hat{y}(t+2|t) = a^2 y_t + b\Delta u_{t+1} - ab\Delta u_t \quad (14)$$

After combining equations (11) and (14), a one and two steps ahead prediction is obtained based on the past input-output and the future input values:

$$\begin{pmatrix} \hat{y}(t+1|t) \\ \hat{y}(t+2|t) \end{pmatrix} = \begin{pmatrix} -a \\ a^2 \end{pmatrix} y_t + \begin{pmatrix} b & 0 \\ -ab & b \end{pmatrix} \begin{pmatrix} \Delta u_t \\ \Delta u_{t+1} \end{pmatrix} \quad (15)$$

The derivation of predictions over additional steps may be done in a similar way, as it is described in Section 2.2.1. Similarly, other models may be used with the same idea of substitution to find the i-step predictions.

2.2.1 Prediction with the state space models

A state space model, permits a multiple step prediction by introducing recursively the one step prediction equation, as shown in [15]:

$$\begin{aligned} x_{t+1} &= Ax_t + Bu_t \\ y_{t+1} &= Cx_{t+1} \end{aligned} \quad (16)$$

For $t+2$

$$\begin{aligned} x_{t+2} &= Ax_{t+1} + Bu_{t+1} \\ y_{t+2} &= Cx_{t+2} \end{aligned} \quad (17)$$

Substituting Equation (16) into Equation (17):

$$\begin{aligned} x_{t+2} &= A^2 x_t + ABu_t + Bu_{t+1} \\ y_{t+2} &= Cx_{t+2} \end{aligned} \quad (18)$$

Repeating the substitution for $t+3$:

$$\begin{aligned} x_{t+3} &= A^2[Ax_t + Bu_t] + ABu_{t+1} + Bu_{t+2} \\ y_{t+3} &= Cx_{t+3} \end{aligned} \quad (19)$$

For the k-step prediction:

$$\begin{aligned} \hat{x}(t+k|t) &= A^k x_t + A^{k-1}Bu_t + A^{k-2}Bu_{t+1} + \cdots + Bu_{t+k-1} \\ \hat{y}(t+k|t) &= C[A^k x_t + A^{k-1}Bu_t + A^{k-2}Bu_{t+1} + \cdots \\ &\quad + Bu_{t+k-1}] \end{aligned} \quad (20)$$

This may be written in matrix form for the prediction horizon N:

$$\underbrace{\begin{bmatrix}\hat{x}_{t+1}\\ \hat{x}_{t+2}\\ \hat{x}_{t+3}\\ \vdots\\ \hat{x}_{t+N}\end{bmatrix}}_{\substack{x\\ \to t+1}} = \underbrace{\begin{bmatrix}A\\ A^2\\ A^3\\ \vdots\\ A^N\end{bmatrix}}_{F_x} x_t + \underbrace{\begin{bmatrix}B & 0 & 0 & \cdots\\ AB & B & 0 & \cdots\\ A^2B & AB & B & \cdots\\ \vdots & \vdots & \vdots & \vdots\\ A^{N-1}B & A^{N-2}B & A^{N-1}B & \cdots\end{bmatrix}}_{H_x} \underbrace{\begin{bmatrix}u_t\\ u_{t+1}\\ u_{t+2}\\ \vdots\\ u_{t+N-1}\end{bmatrix}}_{\substack{u\\ \to t}} \quad (21)$$

$$\underbrace{\begin{bmatrix}\hat{y}_{t+1}\\ \hat{y}_{t+2}\\ \hat{y}_{t+3}\\ \vdots\\ \hat{y}_{t+N}\end{bmatrix}}_{\substack{y\\ \to t+1}} = \underbrace{\begin{bmatrix}CA\\ CA^2\\ CA^3\\ \vdots\\ CA^N\end{bmatrix}}_{F} x_t + \underbrace{\begin{bmatrix}CB & 0 & 0 & \cdots\\ CAB & CB & 0 & \cdots\\ CA^2B & CAB & CB & \cdots\\ \vdots & \vdots & \vdots & \vdots\\ CA^{N-1}B & CA^{N-2}B & CA^{N-3}B & \cdots\end{bmatrix}}_{H} \underbrace{\begin{bmatrix}u\\ \to t\end{bmatrix}}_{} \quad (22)$$

So the prediction for the standard model of Equation (16) is defined as:

$$\begin{aligned} \underset{\to t+1}{x} &= F_x x_t + H_x \underset{\to t}{u} \\ \underset{\to t+1}{y} &= F x_t + H \underset{\to t}{u} \end{aligned} \quad (23)$$

2.2.2 The Free and forced response

The *free* and *forced* response concepts are commonly used in different MPC algorithms. The main purpose is to express the control sequence as the sum of two signals:

$$u_t = u_f(t) + u_c(t)$$

Where the signal $u_f(t)$ is consistent with the past inputs and is maintained constant (equal to the last value) in the future:

$$u_f(t-k) = u(t-k) \text{ for } k = 1,2,\ldots$$

$$u_f(t+k) = u(t-k) \text{ for } k = 0,1,2,\ldots$$

In the case of $u_c(t)$, the values in the past are made equal to zero, and the following time instants are made equal to next control moves in the future:

$$u_c(t-k) = 0 \text{ for } k = 1,2,\ldots$$

$$u_c(t+k) = u(t+k) - u(t-1) \text{ for } k = 0,1,2,\ldots$$

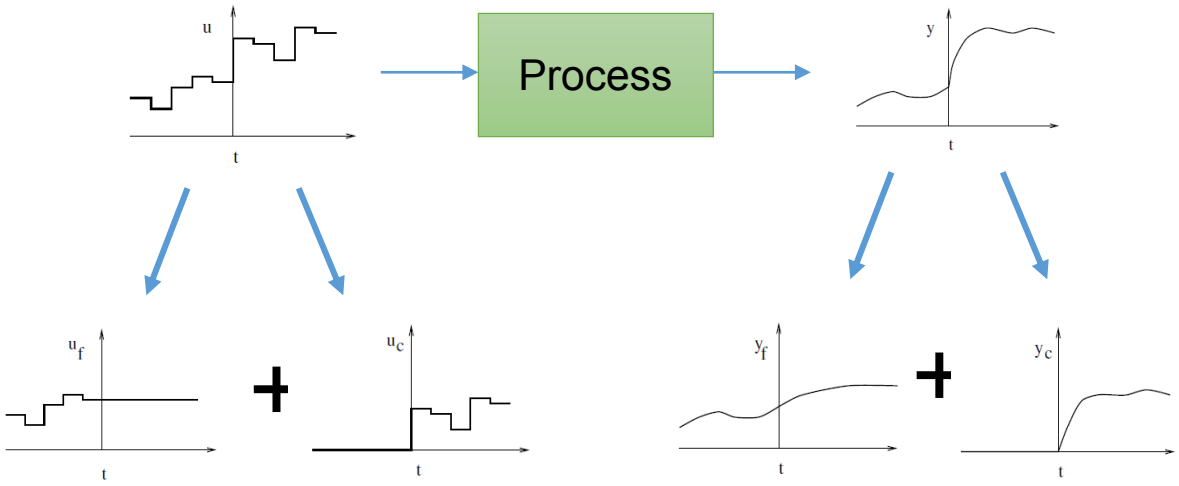

Figure 1. Free and forced response *[12]*

As shown in *Figure 1*. the prediction of the output sequence has been separated in two parts, the *free* response $y_f(t)$, is the forecast of the process when the manipulated variable is equal to $u_f(t)$; and the *forced* response $y_c(t)$, corresponds to the prediction of the process when making the control sequence equal to $u_c(t)$. In other words the *free* response is the evolution of the process, if there are no changes in the manipulated variable in the present state; while the *forced* response is the development of the process due to future control changes.

2.3 Objective Function and Constraints

MPC algorithms make use of varied cost functions to obtain the control law [16]. These algorithms use the objective function to ensure that the outputs follow a fixed reference setpoint in the future until the considered prediction horizon, whereas the necessary control efforts are not too high. Thus, a general expression for the objective function is shown:

$$J = \sum_{i=N_{min}}^{N_{max}} [r_{t+i} - \hat{y}(t+i|t)]^T Q_i [r_{t+i} - \hat{y}(t+i|t)] + \sum_{i=N_{min}}^{N_c} [\Delta u_{t+i-1}]^T R_i [\Delta u_{t+i-1}] \quad (24)$$

The parameters N_{min} and N_{max} are the minimum and maximum prediction horizons, while N_c is the control horizon. N_c may differ from N_{max}. The meaning of the parameters N_{min} and N_{max}, may be intuitively derived. These parameters mark an interval where the reference trajectory is optimal. Therefore if a high value parameter N_{min} is considered, then previous errors are unimportant. If the process possesses a dead time d, then N_{min}should be a larger value than $t + d$. In some instances, where the process has an inverse response, this behavior may be omitted from the objective function. Q_i and $R_i$are the weighting matrices.

The reference trajectory is the desired direction that must be followed by the process. Even though it is preferred that the process output will reach the setpoint with no errors, there might be differences with the actual output of the process due to model mismatch, time delays or some hard constraints. It is common to use a smooth curve starting from the current value of the output and approaching the setpoint as the reference trajectory.

Processes are limited to certain constraints. For instance, actuators need specific restrictions that prevent them from going beyond their physical limits. Other constraints are imposed due to economic and safety reasons. For example, a chemical reaction may be favored at high temperatures, but the reactor may have a definite threshold which should not be surpassed, due to material tolerance and safety reasons. MPC considers integrating constraints, and this inclusion has been demonstrated to be successful in industry. In general the constraints present the following formulation:

$$\begin{aligned} u_{min} \leq u_t \leq u_{max} \quad & \forall t \\ du_{min} \leq u_t - u_{t-1} \leq du_{max} \quad & \forall t \\ y_{min} \leq y_t \leq y_{max} \quad & \forall t \end{aligned} \tag{25}$$

With the inclusion of these constraints to the optimization, calculations become more complex. However, this allows MPC to control the process according to the restrictions existing in the applications.

2.4 Control Law

The input of the process, or control actions Δu_{t+i}, are computed by minimizing the objective function. For this purpose, the output prediction $\hat{y}(t+1|t)$ is calculated, for example as shown in Equation (15), and used to compute the objective value according to Equation (24). Subsequently a derivative of the cost function is taken with respect to Δu_t, Δu_{t+1},…, Δu_{t+N_c-1}, and the solution of the optimization is found by equating the derivatives to zero. By following this algorithm, which is a typical least squares problem, it is possible to obtain an analytical solution.

If some constraints exist on u_t, Δu_t, or $\hat{y}(t+1|t)$, analytical solutions are no longer possible, and some numerical minimization is needed. It is important to remember that all these calculations occur within the sampling time interval.
The control horizon serves as a means to impose a structure on the control law, as u_t becomes constant after it:

$$\Delta u_{t+i-1} = 0 \quad i > N_c \tag{26}$$

2.5 Review of MPC Algorithms

This section presents a short description of some of the most popular MPC methods used in industry, with the purpose of demonstrating the most important characteristics.

2.5.1 Dynamic Matrix Control

The Dynamic Matrix Control (DMC) method, assuming that the process is stable and with no integrators, employs the step response model (2), and considers the first N terms. The disturbances are assumed to be equal to the measured value of the output y_m minus the value predicted by the model $\hat{y}(t|t)$.

$$\hat{d}(t+k|t) = \hat{d}(t|t) = y_m - \hat{y}(t|t) \tag{27}$$

The predicted output value becomes:

$$\hat{y}(t+k|t) = \sum_{i=1}^{k} g_i \Delta u_{t+k-i} + \sum_{i=k+1}^{N} g_i \Delta u_{t+k-i} + \hat{d}(t+k|t) \tag{28}$$

The first term on the right hand side of the previous equation contains the future control actions to be calculated, while the second term are the past input values, which is known information, and the last term represents the disturbances.

The cost function considers either simply future errors, or may include the control effort as well, as defined by Equation (24). Furthermore, it is possible to add some constraints to this method, with a general form:

$$\sum_{i=1}^{N} C_{yi}^{j} \hat{y}(t+k|t) + C_{ui}^{j} u(t+k-i) + c^{j} \leq 0 \quad j = 1 \dots N_C \tag{29}$$

Afterwards, numerical optimization must be performed at every sampling instant, and the value of u_t, is sent to the process in a similar way with to all MPC methods. There are a few disadvantages with this method, such as: in presence of unstable processes the method is not applicable, and the required size of the process model.

2.5.2 Model Algorithmic Control

Marketed under the name IDCOM (Identification-Command), also known as Model Predictive Heuristic Control, this method presents many similarities with respect to DMC. The main difference of IDCOM is the use of an impulse response model (1), thus, the value of Δu_t is replaced with u_t in the modeling equations. Similarly to DMC, this method is also effective only for stable processes. This method does not use the idea of a control horizon. Instead it introduces a reference trajectory continuously changing from the latest output value towards the setpoint. The trajectory is generated by a first order system with a certain time constant [12]:

$$w_t = y_t \qquad (30)$$
$$w_{t+k} = \alpha w_{t+k-1} + (1-\alpha) r_{t+k} \quad k = 1 \dots N$$

The parameter α is given a value between 0 and 1, and it is a value that may be modified to influence the dynamic response of the system.

The objective is to minimize the difference between the trajectory and the output. In MAC the disturbances may be handled similarly compared to DMC, or it is possible to make an estimation using the recursive expression:

$$\hat{d}(t+k|t) = \alpha \hat{d}(t+k-1|t) + (1-\alpha) y_m - \hat{y}(t|t) \qquad (31)$$

With $\hat{d}(t|t) = 0$. The parameter α is adjustable, as stated before ($0 \leq \alpha < 1$), and is directly related to the bandwidth, the response time, and the robustness of the closed loop system [17].

2.5.3 Predictive Functional Control

This method was developed for the implementation of fast processes [18]. This strategy includes a state space model of the process and allows the use of nonlinear and unstable linear models. The nonlinear dynamics are introduced to the PFC as a nonlinear state space model. PFC features two important characteristics: the implementation of coincidence points and basis functions.
Coincidence points are used to make the calculation simpler, by only taking in consideration a subset of values in the prediction horizon. It is only required that the setpoint and predicted future outputs, concur at these points and not over all the prediction horizon. The second characteristic is the utilization of polynomial basic functions in order to parametrize the control signal. These functions are defined as:

$$u_{t+k} = \sum_{i=1}^{n} \mu_i(t) B_i(k) \qquad (32)$$

The values of B_i are selected depending on the nature of the process and the reference, which are commonly polynomials.

$$B_0 = 1, \;\; B_1 = k, \;\; B_2 = k^2, \ldots$$

This property permits the use of a small number of parameters to specify a relatively complex input over a considerably large horizon. These functions may be defined with certain specifications, for instance in mechanical servo control applications, they may be used to follow a polynomial setpoint with no lag.

In PFC the cost function to be minimized is defined as follows:

$$= J \sum_{j=1}^{n_H} \left[\hat{y}_{t+h_j} - w_{t+h_j}) \right]^2 \qquad (33)$$

Where w is generally a first order approach to the reference. It is also possible to include maximum and minimum input acceleration constraints to the PFC algorithm, this is convenient for the servo control applications [12].

2.5.4 Generalized Predictive Control

The GPC algorithm makes use of the CARIMA (Controlled Auto Regressive Moving Average) model:

$$A(z^{-1})y_t = B(z^{-1})z^{-d}u_{t-1} + \frac{C(z^{-1})e_t}{\Delta} \qquad (34)$$

It is possible to obtain the optimal prediction by solving a Diophantine equation, this solution is found with the help of an efficient recursive algorithm.
The cost function of GPC is quadratic:

$$J(N_1, N_2, N_u) = \sum_{i=N_{min}}^{N_{max}} \delta_i[\hat{y}(t+i|t) - w_{t+i}]^2 + \sum_{i=1}^{N_c} \lambda_i[\Delta u_{t+i-1}]^2 \qquad (35)$$

Where δ_i and λ_i are weighting sequences, which are normally selected as constant or exponentially increasing, while w_{t+i} is the reference trajectory and is normally generated, with a simplified recursion, beginning from the current value of the output and moves exponentially towards to the setpoint.
This algorithm has been studied broadly in the past, and it has been shown that, for a small number of the parameter choices, this algorithm is stable [19].

2.6 Stabilizing Model Predictive Control:

From here onwards the set theory notation will be put in use for better understanding of the topic. This notation is widely used in the field of advanced control strategies.

Considering the nonlinear system to be of the form:

$$x_{t+1} = f(x_t, u_t), \qquad x_0 = x(0) \tag{36}$$

Where $f: \mathbb{X} \times \mathbb{U} \to \mathbb{R}^n$, $u_t \in \mathbb{U} \subseteq \mathbb{R}^m$, and $x_t \in \mathbb{X} \subseteq \mathbb{R}^n$ are the control input and system state respectively, with time $t \in \mathbb{I}_{\geq 0} = [0,1,2 \dots]$, and initial condition $x_0 \in \mathbb{X}$. The constraints for the system may be expressed as:

$$(x_t, u_t) \in \mathbb{Z} \subseteq \mathbb{X} \times \mathbb{U} \tag{37}$$

For all $t \in \mathbb{I}_{\geq 0}$; denote by $\mathbb{Z}_{\mathbb{X}}$ the projection of $\mathbb{Z}$ on $\mathbb{X}$, in other words:

$\mathbb{Z}_{\mathbb{X}} \coloneqq \{x \in \mathbb{X}: \exists u \in \mathbb{U}, (x,u) \in Z\}$. S is delimited as the set of all feasible state/input equilibrium pairs of Equation (36):

$$S \coloneqq \{(x,u) \in \mathbb{Z}: x = f(x,u)\}, \tag{38}$$

The set S is assumed to be non-empty. The control for the system in Equation (36) should be stabilized at a setpoint x^*, this value is a point of the system, where it lies in equilibrium. The corresponding control input is u^*, this means: $(x^*, u^*) \in S$. The following assumption are taken: The function f is considered as continuous, the set $\mathbb{U}$ is compact, and the set $\mathbb{Z} \subseteq \mathbb{X} \times \mathbb{U}$ is closed.

The following optimization problem is solved, with the purpose of defining the receding horizon control law at every time $t \in \mathbb{I}_{\geq 0}$, the state x_t is measured.

$$\begin{gathered} \min_{u_t} J_N(x_t, u_t) \\ \hat{x}(t+1|t) = f(x_t, u_t), \qquad t \in \mathbb{I}_{[0,N-1]} \\ x_0 = x(0) \\ (x_t, u_t) \in \mathbb{Z}, \quad t \in \mathbb{I}_{[0,N-1]} \\ x_N = x(N) \in \mathbb{X}^f \end{gathered} \tag{39}$$

Where:

$$J_N(x_t, u_t) \coloneqq \sum_{i=0}^{N-1} \ell(x_t, u_t) + V^f(x_N) \tag{40}$$

The closed terminal region is defined as $\mathbb{X}^f \subseteq \mathbb{X}$, also the stage cost function is $\ell: \mathbb{X} \times \mathbb{U} \to \mathbb{R}$ and the terminal cost function $V^f: \mathbb{X}^f \to \mathbb{R}$. These functions are assumed to be continuous.

Denoting the values that minimize the cost function:

$$\underset{\to 0}{u^0} \coloneqq [u^0(0|t), \dots, u^0(N-1|t)]$$

the corresponding state sequence:

$$\underset{\to 0}{x^0} \coloneqq [x^0(0|t), \dots, x^0(N-1|t)]$$

and the corresponding optimal value function:

$$J_N^0(x_t) \coloneqq J_N\left(x_t, \underset{\to 0}{u^0}\right) \tag{41}$$

Now the MPC may be solved with the following algorithm:

1- Consider the system of Equation (36)
2- Measure the state x_t at each time $t \in \mathbb{I}_{\geq 0}$
3- Solve problem of Equation (39)
4- Apply control input $u_t \coloneqq u^0(0|t)$

The results of the algorithm in the closed loop system are:

$$x_{t+1} = f\big(x_t, u^0(0|t)\big), \quad x_0 = x(0) \tag{42}$$

With purpose of guaranteeing that x^* is a stable equilibrium point for the system in Equation (42), some condition should be imposed on the stage and terminal cost functions (ℓ, V^f), and terminal region $\mathbb{X}^f$ [11].

The stage cost function ℓ satisfies $\ell(x^*, u^*) = 0$, and there exists a function $\alpha_1 \in \mathcal{K}_\infty$ such that $\ell(x_t, u_t) \geq \alpha_1(|x - x^*|)$ for all $(x_t, u_t) \in \mathbb{Z}$. Furthermore the terminal cost function V^f satisfies $V^f(x^*) = 0$ and $V^f(x) \geq 0, \quad \forall x \in \mathbb{X}^f$.

The terminal region $\mathbb{X}^f \subseteq \mathbb{X}$ is closed and $x^* \in \mathbb{X}^f$. Additionally there is a local auxiliary control law such that $u_t = \kappa^f(x)$ and for all $x \in \mathbb{X}^f$ the following is satisfied:

i) $(x, \kappa^f(x)) \in \mathbb{Z}$

ii) $f(x, \kappa^f(x)) \in \mathbb{X}^f$

iii) $V^f(f(x, \kappa^f(x))) - V^f(x) \leq -\ell(x, \kappa^f(x)) + \ell(x^*, u^*)$

The previous assumption denotes that when the local auxiliary controller is implemented to the system in Equation (36), i) input and state constraints are fulfilled inside the terminal region and ii) the terminal region is invariant. Condition iii) signifies that V^f serves as a Lyapunov function included in the terminal region (for this case V^f is positive with respect to x^*). These assumptions are considered standard for stabilizing in MPC with a terminal cost/ terminal region setting [11].

Denoting $\mathbb{X}_N$ as the set of all states $x \in \mathbb{X}$, such that the system in Equation (36), has a solution. Supposing that all assumptions hold, then the system is feasible for all $t \in \mathbb{I}_{\geq 0}$. Additionally for the closed loop system that results from the previous algorithm, the input constraints and the pointwise-in-time state are satisfied for all $t \in \mathbb{I}_{\geq 0}$, and x^* is an equilibrium point asymptotically stable with region of attraction $\mathbb{X}_N$ [11].

3 Economic Model Predictive Control:

Through the years MPC became more popular in industry and for academic research. The combination of MPC with Real Time Optimization (RTO) as shown on the left side of Figure *2*, has become a classical control approach in industries [20]. The RTO, determining the economically optimal setpoint for the process, is generally done in a timeframe of hours at a specific steady state [21]. The setpoint is sent to the second layer, in this case the MPC, and the controller drives the process to the setpoint provided by the RTO. The drawback of this two-layer approach is that the RTO focuses on the steady-state optimization, which may not necessarily be the economically best strategy. This is caused by the possible presence of an unreachable set point obtained from the economic optimization [22].

It was discovered that economic optimization may be considerably improved if the cost function were to be incorporated directly into the MPC [23] [24]. Economic Model Predictive Control (EMPC) is a variation of MPC, which uses a general cost function to dynamically optimize the process economy [25]. In this case, no reference or a target steady state is provided to the EMPC, and the objective function is not necessarily positive definite as commonly accepted for the standard MPC [26]. The control structure relying on EMPC is shown on the right side of Figure *2*.

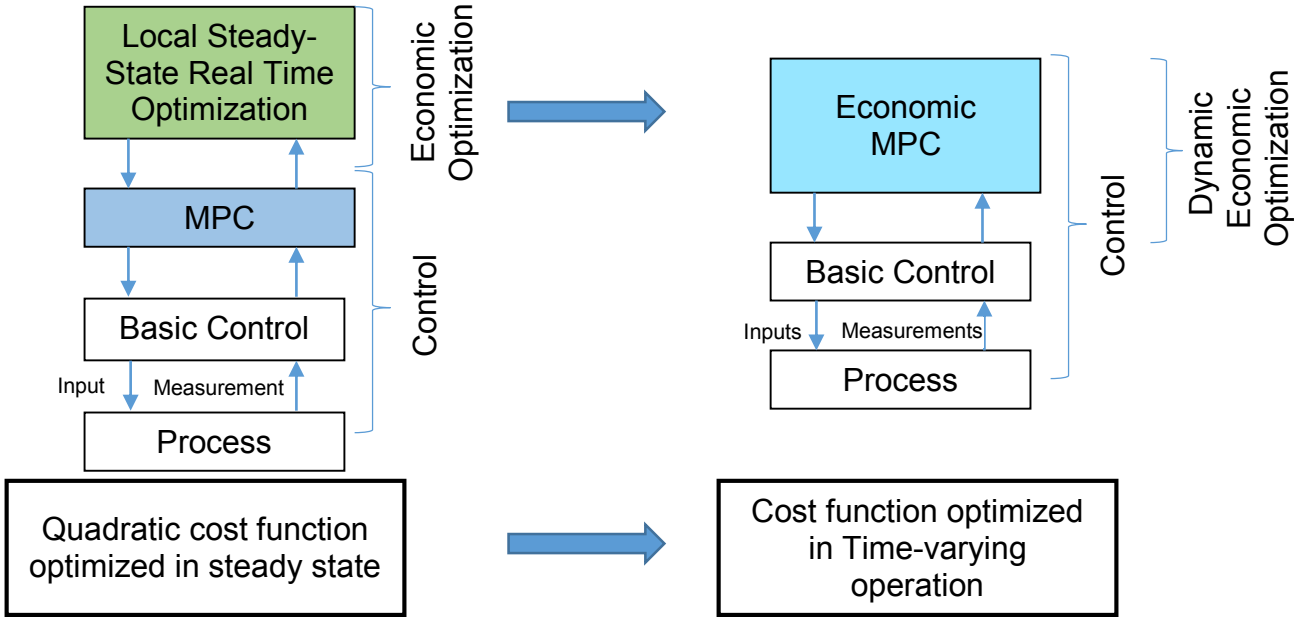

Figure *2. Differences between MPC with RTO and EMPC* [4]

Currently, EMPC has already become a well-established technique with a range of implementations [27]. Similar to the MPC optimization, the EMPC objective is defined as follows:

$$J_N(x_t, u_t) := \sum_{i=0}^{N-1} \ell(x_t, u_t) \tag{43}$$

where the stage cost function $\ell(x_t, u_t)$ defined as an arbitrary cost function that resembles the economics related to the process [28]. Similarly to traditional MPC, the stage cost function is commonly convex for linear systems and frequently non-convex for non-linear systems.

In contrast to the traditional MPC, the stage cost function $\ell(x_t, u_t)$ from Equation (43), may not achieve its minimum at a fixed equilibrium state. In other words, the optimal steady state stage cost for MPC is not necessarily smaller compared to the stage cost in EMPC. Therefore, limit cycles may arise in EMPC because they are economically favorable, which can only happen for a nonlinear process

dynamics or a nonconvex economic objective. Therefore, it is desirable to reach the following asymptotic average limit:

$$\limsup_{T\to+\infty} \frac{\sum_{t=1}^{T} \ell(x_t, u_t)}{T} \leq \ell(x_S, u_S) \tag{44}$$

In order to ensure the average EMPC performance, as defined by Equation (37), denote the decision vector $\underset{\to 0}{u} \coloneqq [u(0|t), \dots, u(N-1|t)]$ to be the control sequence for each time step calculated for MPC, as stated before. Next, consider the admissible set $\mathbb{Z}_N$ of $\left(x_0, \underset{\to 0}{u}\right)$ pairs that satisfies the following constraints

$$\mathbb{Z}_N \coloneqq \begin{Bmatrix} \left(x_0, \underset{\to 0}{u}\right) | \exists x_1, \dots, x_N : x_{t+1} = f(x_t, u_t), \\ (x_t, u_t) \in \mathbb{Z}, t \in \mathbb{I}_{[1,N-1]} \\ x_0 = x(0), x_s = x_N \end{Bmatrix}, \tag{45}$$

and its projection $\mathcal{X}_N$ on $\mathbb{X}$ that is defined as:

$$\mathcal{X}_N \coloneqq \left\{ x \in \mathbb{X} \,\middle|\, \exists \underset{\to 0}{u} : \left(x, \underset{\to 0}{u}\right) \in \mathbb{Z}_N \right\}. \tag{46}$$

According to [3], for any $x \in \mathcal{X}_N$ exists at least one control sequence that directs the state to x_S at time N without abandoning $\mathcal{X}_N$ and the closed-loop system in (36) with $\underset{\to 0}{u}^0$ has an asymptotic average performance that is, as a minimum, as suitable as the best admissible steady state.

Even though the asymptotic average performance is assured, the EMPC with objective defined by Equation (43) does not guarantee the stability in closed loop. In traditional MPC, the optimal cost of $J_N(x_t)$, denoted before as $J_N^0(x_t)$ in Equation (41) is used as a Lyapunov function for the closed loop system, as it is monotonically decreasing for different closed loop solutions, meaning that $J_N^0(x_{t+1}) \leq J_N^0(x_t)$. However, for EMPC, this does not necessarily occurs because of the possible limit cycles, even if the system is stable. The reason for that is that in the case of non-convex cost functions and general nonlinear systems, it is not guaranteed that x_S is the optimal steady state.

However, convergence to a steady-state can be ensured for an EMPC with the terminal constraint using a Lyapunov function, if the strong duality assumption is satisfied [29], meaning that the solution x_s, u_s of the steady state optimization problem

$$\begin{aligned} &\min_{x,u} l(x,u) \\ &x = f(x,u) \\ &g(x,u) \leq 0 \end{aligned} \tag{47}$$

is the only minimizer of the following expression for some Lagrange multiplier λ_s:

$$\min_{x,u} l(x,u) + \big(x - f(x,u)\big)' \lambda_s. \tag{48}$$

Later, the strong duality condition (47), (48) was relaxed to the dissipativity assumption [24].

The system of Equation (36) is said to be dissipative with respect to the supply rate $s(x_t, u_t): \mathbb{X} \times \mathbb{U} \to \mathbb{R}$, If a function $\lambda: \mathbb{X} \to \mathbb{R}$ exists, such that:

$$\lambda\big(f(x_t, u_t)\big) - \lambda(x_t) \leq s(x_t, u_t), \forall (x_t, u_t) \in \mathbb{Z} \tag{49}$$

Additionally, if a function $\rho: \mathbb{X} \to \mathbb{R}_{\geq 0}$, positive definite exists, such that:

$$\lambda\big(f(x_t, u_t)\big) - \lambda(x_t) \leq -\rho(x_t) + s(x_t, u_t), \tag{50}$$

Then it is said that the system is strictly dissipative [3].

There are several formulations to achieve closed-loop stability if the dissipativity assumptions are fulfilled, including the terminal constraints and the terminal costs.

For the economic problem, the closed loop system x_S is an asymptotically stable point with region of attraction $\mathcal{X}_N$, if it is strictly dissipative with respect to the supply rate in Equation (49), (50). This can be proven by creating an auxiliary augmented problem with a rotated stage cost, subsequently showing that the feasible sets, $\mathcal{X}_N$, coincide. Finally it exhibits that the objective function of the

original and rotated formulations are different only by a constant, concluding that both solutions are the same [3].

Stability in the closed-loop may also be achievable by employing an adequate terminal cost with an inequality terminal constraint, as opposed of an equality constraint. This proof also involves a rotated stage cost, which is considered as a Lyapunov function, and taking into consideration the strict dissipativity property [3].

4 Calcination of kaolin

This chapter provides a general view of the kaolin processing, and afterwards it focuses on the calcination process which is the interest of this work.

4.1 Kaolin processing

Kaolin clays are commonly extracted from open pits, because underground mining involves added costs of production that may not be optimal or in some cases prohibitive, for a stable operation. Ore obtained from the deposits needs to be refined since the mineral contains many impurities and the kaolin calcining stage requires high quality kaolin as raw material for processing. The kaolin is extracted from the pits with a method known as wet processing giving a more efficient extraction compared to dry processing [30]. Wet processing yields higher uniformity, improved color and the mineral is relatively free of impurities. The processing of the clay generates large quantities of by-products. These include rock, mica and sand. In Figure 3 a simplified view on the kaolin extraction, refining and processing is presented.

The flow of kaolin from the pit to the calcining stage is classified into three main stages:

I. Pit operations
II. Refining processes
III. Drying processes

After the kaolin passes through these stages it is ready to be calcined.

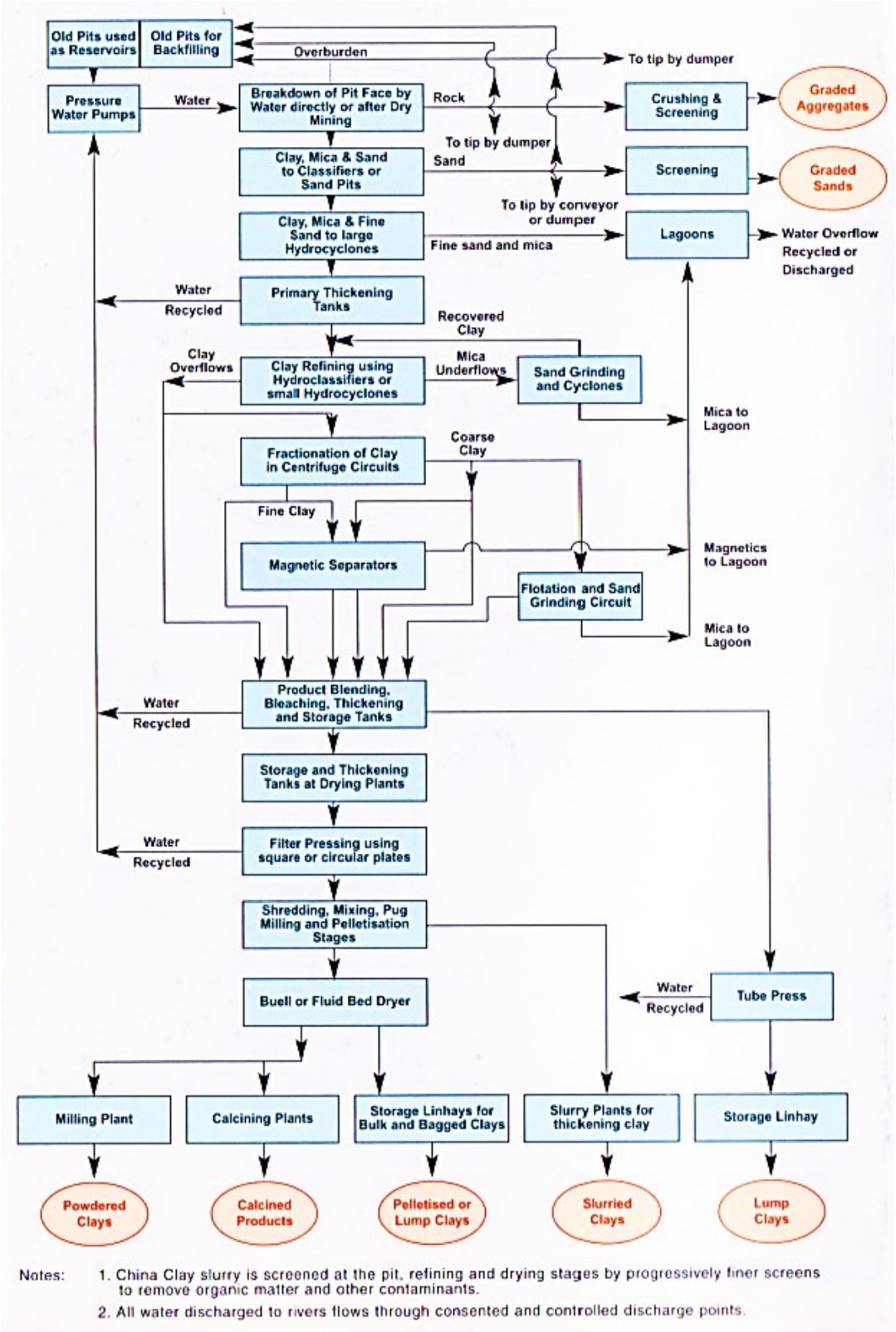

Figure 3. Simplified flow diagram of kaolin production [30]

4.2 Kaolin Calcination

Calcination is a very important unitary operation that is used to process solids in order to yield a value-added product. Calcination was introduced in the beginning of the 1950s [31]. The calcination process contributes to an increase in hardness and modifies the structure of the kaolin. The calcination provides kaolin a low dielectric loss due to the lack of crystallinity, and an excellent insulation performance. This process effectively upgrades opacity, brightness and other characteristics of kaolin. Furthermore, calcined kaolin has diverse industrial applications such as the paint industry, paper industry, pharmaceutical industry, and many others.

Calcined kaolin may be classified generally in two grades. The first grade corresponds to a kaolin with improved brightness and opacity. This kaolin grade is treated at temperature between 450 to 700 °C [32]. The product has a bulky characteristic and may be used as coating additive for paper, to increase resiliency and opacity in low basis weight sheets [33].

Further heating of kaolin to a temperature close to 980 °C causes a physicochemical change that transforms the amorphous mixture of alumina and silica to a more organized structure, giving rise to the stage known as “spinel phase” [34]. If the material is heated even more, it causes a new modification, where the spinel phase forms high temperature quartz, also known as cristobalite, and small crystals of mullite [35]. The second grade of calcined kaolin is constituted by spinel phase and mullite, which has a brightness between 92 and 94% [32]. The second grade of calcined kaolin is whiter with an increased abrasivity, compared to the primary kaolin [36]. The mullite content in the kaolin determines the abrasivity, with high concentrations of mullite the product will be more abrasive. The abrasivity is controlled by selecting a proper feed of kaolin, maintaining acceptable temperatures during calcination, and appropriate

processing after calcination. The following *Table 1* describes the differences between the two calcination grades for kaolin.

Table 1. Kaolin grades and changes in properties *[37]*.

Kaolin	Calcination (grade 1)	Calcination (grade 2)
Brightness	Increased	Increased
Particle shape	Changed	Changed
Particle size	Changed	Changed
Opacity	Improved	-
Color	-	Whiter
Abrasion	-	Increased
Specific surface area	-	Increased
Temperature range	500-700 °C	1000-1100 °C
Porosity	Increased with higher temperatures	

The following set of equations describe the different physicochemical transformations that kaolin suffers during calcination [38]:

I. Dehydroxylation of kaolinite to metakaolinite:

$$Al_2O_3 \cdot 2SiO_2 \cdot 2H_2O \overset{450-700°C}{\Longrightarrow} Al_2O_3 \cdot 2SiO_2 + 2H_2O_{(g)} \quad (51)$$

II. Formation of Al–Si spinel phase from metakaolinite

$$2(Al_2O_3 \cdot 2SiO_2) \overset{925-1050°C}{\Longrightarrow} 2Al_2O_3 \cdot 3SiO_2 + SiO_{2(\text{amorphous})} \quad (52)$$

III. Formation of mullite

$$3(2Al_2O_3 \cdot 3SiO_2) \overset{\geq 1050°C}{\Longrightarrow} 2(3Al_2O_3 \cdot 2SiO_2) + 5SiO_2 \quad (53)$$

IV. Crystallization of cristobalite from amorphous silica

$$SiO_{2(\text{amorphous})} \overset{\geq 1200°C}{\Longrightarrow} SiO_{2(\text{cristobalite})} \quad (54)$$

At the beginning free water is removed by evaporation at temperature near 100 °C. There, the energy is absorbed as latent heat due to the evaporation. In the first reaction (51) a loss of weight (Dehydroxylation) occurs which is displayed in the thermogravimetric (TG) curve shown in *Figure 4* [39]. The reaction is endothermic as determined by differential scanning calorimetry (DCS) curve presented in the blue line of the same figure. The second (52) reaction, depicted in the temperature range 925-1050°C, is exothermic. In the second reaction (52), the crystal structure of the metakaolin transmutes to a more stable state, and a part of solid transforms into mullite in the third reaction (53) [40]. The fourth reaction (54) only occurs when further heating is applied to over 1200 °C, which in this particular process is not performed.

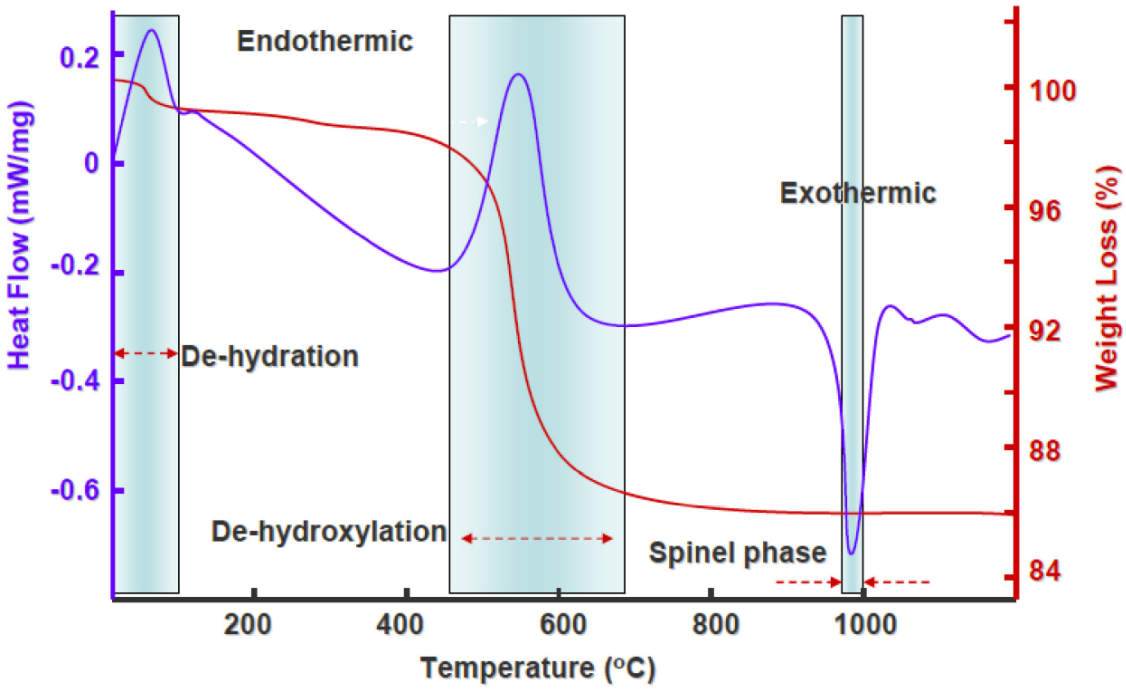

Figure 4. Thermogravimetric analysis and Differential Scanning Calorimetry Curve for kaolin calcination (provided by IMERYS).

4.3 Review of control strategies for the MHF

4.3.1 Fuzzy logic control for Nickel Recovery Process

One of the areas where MHF has been employed is the selective reduction of nickel. The MHF configuration considered in this section is installed at the Nicaro plant in Cuba. The configuration of this particular MHF is illustrated in Figure 5. The furnace dimensions are 6.7 m in diameter and 21.3 m high, contains 17 circular hearths, numbered top to bottom from the H-0 until the H-16. The reductant is dried ore and blended with fuel oil, previous to the feed to the roaster, where it is roasted at 700–800 °C with a 5400 s of retention time. The ore is also warmed up by the hot reducing gas (CO + H_2). This gas is generated in nine combustion chambers positioned along the furnace. The combustion of the fuel oil occurs in a deficiency of air. The chemical heat value of the gas is recovered by burning it with the incorporation of secondary air to the hearths 4 and 6. This process is defined as post-combustion. The post-combustion allows a reduction of fuel use by 50%, in this way the furnace consumes about 10 million kilograms of fuel oil per year [41].

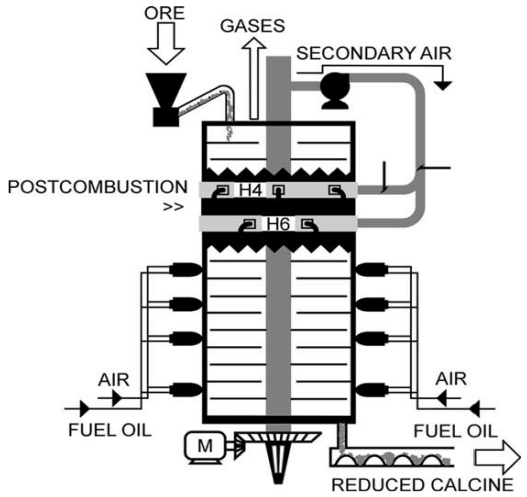

Figure 5 MHF furnace used for Nickel recovery [26]

The effect of the air flow on the steady state temperature in the hearth 4 is notably nonlinear. Moreover, there are actually two operation regions with opposite gain signs. The curve describing the effect of the air flow on the temperature depends on the furnace operating conditions (quantity of carbon in the fed mineral, concentration of reductants in H-4, mineral flow, etc.), as shown in Figure 6.

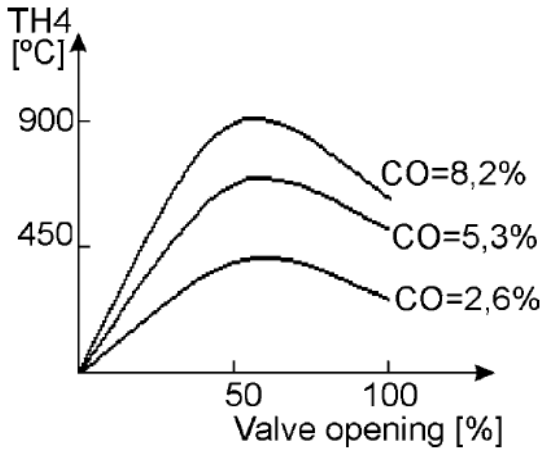

Figure 6 Relationship between the temperature and the air flow of H-4. [26]

It is also widely recognized that this kind of process is hard to control, because it has a rather stochastic nature; it is time-varying, multivariable with interactive influences, and also non-linear. In particular, the traditional PID controllers are not able to perform well due to the gain sign change in the air flow effect on the gas temperature.

To achieve the control objectives, a fuzzy logic controller is designed and implemented in [41]. In more details, a multivariate controller is designed to controls the temperatures in the hearth 4 where the post-combustion process happens. This controller is installed in the supervisory system of a nickel reduction furnace.

Table 2. Elements of the control structure [41]

Control schemes	Manipulated variable	Controlled variable
Fuzzy Controller	Air flow to hearth 4 ($faH4$)	Temperature of hearth 4 ($TH4$)
	Air flow to hearth 6 ($faH6$)	
	Fuel oil flow (fp)	Temperature of hearth 6 ($TH6$)
	Ore flow fed to the roaster (fm)	

The fuzzy controller considers five variables: the control error (e) of temperatures $TH4$ and $TH6$, the change of these errors (ce), and the specific fuel consumption defined as amount of fuel in kilograms used per 1 ton of ore fed to the furnace. While the manipulated variables include the change in airflow to the hearth 4 and 6, fuel oil flow to combustion chambers (fp), and the ore feed rate to the roaster (fm). Mathematically, the considered variables are expressed by:

$$e(k) = r(k) - y(k)$$
$$ce(k) = e(k) - e(k-1) \quad (55)$$

where r is the reference signal, y is the output (of the process), and k is the discrete time, while the final control signal is given by:

$$u(k) = u(k-1) + \Delta u(k). \quad (56)$$

After assigning the membership functions to the variables, the subsequent task is to design the knowledge base. The knowledge bases were created from the experienced operators and control engineering knowledge, i.e., using the so called verbalization technique. Taking into account various regions of operation of the MHF and/or technological restrictions, 60 rule bases were designed, each consisting of 108 rules. A typical rule, for example, is tabulated in Table 3.

Table 3 Example rule base, where A $implies$ B ($A \rightarrow B$) [41]

Rules	A	B
R	$eth4$ is “negative”, and $ceth4$ is “negative”, and $eth4$ is “negative”, and $ceth4$ is “negative”, and $fuel\ comsumption$ is “low”.	$fah4$ is “diminish”; $fah6$ is “augment”; fp is “augment much”; fm is “maintain”.

Number of field tests were performed at the plant. During the tests the process was subject to different disturbances, and the controller maintained the temperature of the hearths H-4 and H-6 in the desired range in all the cases.

4.3.2 Predictive control for recovery of the vanadium process

Rotary Kilns or Multiple Hearth Roasters are commonly used for extraction of Vanadium from steelworks slag. The slag is roasted under alkaline conditions, usually using $NaCl$ or/and Na_2CO_3 as additives. The following chemical reactions are reported in the literature for the conversion of Vanadium

$$\begin{aligned} V_2O_3 + O_2 &\rightarrow V_2O_5 \\ V_2O_5 + 2NaCl + H_2O &\rightarrow 2NaVO_3 + 2HCl \\ V_2O_5 + NaCO_3 &\rightarrow 2NaVO_3 + CO_2 \end{aligned} \qquad (57)$$

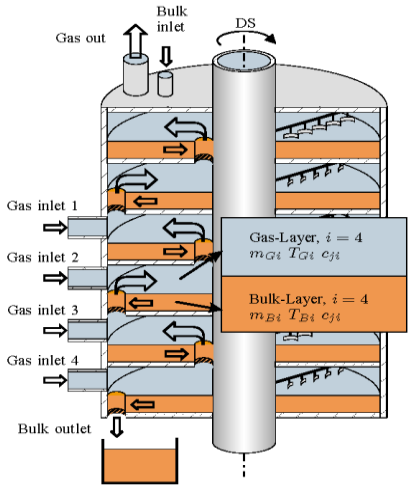

Figure 7 Scheme of a Multiple Hearth Furnace [28]

Figure 7 shows a scheme of the multiple hearth furnace, where $m_{Gi}(t)$ and $m_{Bi}(t)$ are the mass of the bulk (B) and the gas (G) in the hearth i, $T_{Gi}(t)$ and $T_{Bi}(t)$ are the temperature of the gas and the solid, and $c_{ji}(t)$ is the concentrations for the component j on the ith floor. The slag and the additives are fed at the top of the furnace and transported from floor to floor by the shaft driven (DS) agitator. Heat and oxygen are provided in some of the floors by burners with a high excess air.

Assuming homogenous gas- and bulk-layers in every floor, a physically based model of the vanadium roast process in a multiple hearth furnace is derived in [42]. This development yields a nonlinear state space model for calculating the mean values for mass, temperature and concentrations. Further, this nonlinear model is linearized around a typical operating point to facilitate the controller design. It has been observed that the process model order is quite high due to several decisive states on every floor of the MHF. Model order reduction was then carried out by assuming a lower order transfer function structure.

The control objective is to maintain an oxidizing atmosphere during roasting which is essential for maximum efficiency in the conversion of the vanadium. Furthermore, the second control objective is to achieve accurate temperature control in the roasting units which is required for reasonable recovery of the vanadium and to avoid any undesirable process behavior like hearth build up (see [43] and the references therein). To achieve the aforementioned objectives, the overall controller design is divided into four parts. Figure 8 illustrates the block diagram of the controller structure [44]. The main control loops include:

1. pH-control: The pH-value of the roasted bulk is controlled by u_{pH}, the mass flows $\dot{m}_{NaCl}$ and/or $\dot{m}_{Na_2CO_3}$.
2. c- control: Stationary control of a key component concentration by u_c. This system is of minor importance from the control engineer's viewpoint since in practice this control operates in a time scale which is slower compared the process dynamics. Therefore, the design of this controller will not be further discussed.
3. T-control: The temperature T of the individual floors is controlled by the burner gas flow u_T
4. $Overhead$-control: The overhead controller provides the setpoint values for pH w_{pH}, concentration w_c, and temperature w_T to the above control loops.

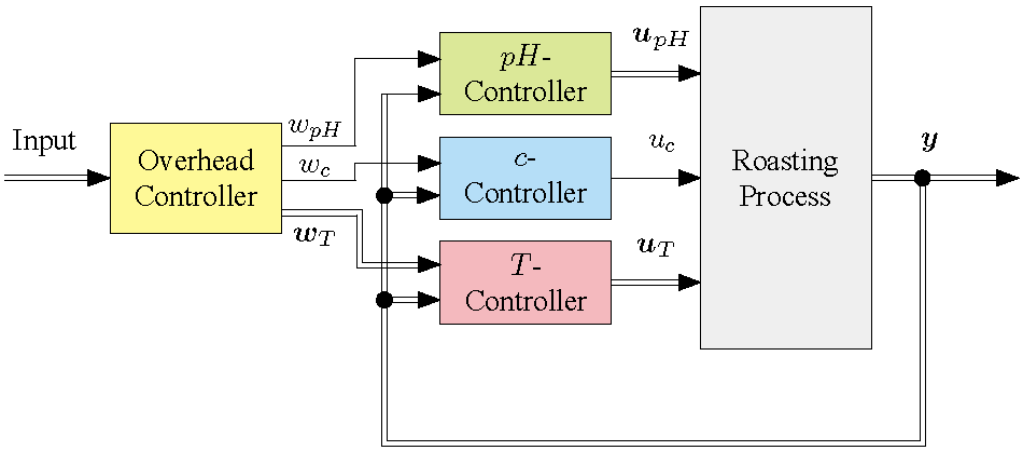

Figure 8 Block diagram of the controller structure [43]

The main aim of designing the temperature controller is to maintain a desired temperature profile over the furnace by controlling the temperature of the individual floors. This usually gives a strongly coupled multivariable system. In the preliminary works of [43], PI controllers were designed using the following transfer function:

$$G_{PI} = K\frac{s+a}{s}. \tag{58}$$

The parameters of the controllers were selected by optimizing a quadratic cost functional, including the tracking error and the weighted control efforts.

Concerning the pH-control, a total dead time T_{pH} is composed of the retention time and the time of the offline analysis of the pH-value. Consequently, a Smith predictor control structure is employed, as illustrated in Figure 9. In this predictive control scheme, the knowledge of the process model G_P and a precise information of the total dead time is required to estimate the $\widehat{pH}$ value. The sampled and delayed variable $pH_{meas.}$ is used to compensate modelling errors or the influence of unaccounted disturbances $Z_1, \cdots, Z_m$. Other free variables are the measurable disturbances. Consequently, further improvements in the controlled behavior may be achieved by feed forward controllers.

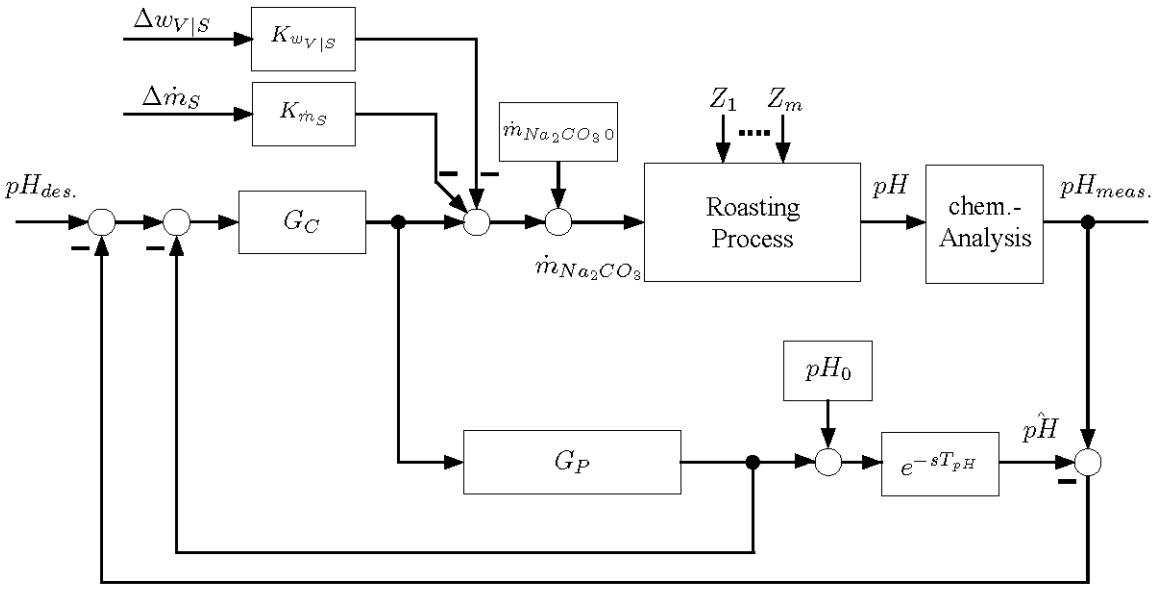

Figure 9 Block diagram of the $\boldsymbol{pH}$-control system with Smith-Predictor [43]

The overhead controller acts with the purpose of enhancing the process efficiency by providing the reference values to the internal closed-loops. In addition, operators take care on the controller to avoid undesirable operating conditions.

4.3.3 Model predictive control for Nickel recovery in the MHF

A multi-variable model predictive control (MPC) technique is used as an advanced process control method to control and optimize a set of nickel reduction roasters located at Votarantim Metais Niquel (VMN) in Niquelandia, Gioas State, Brazil [45]. The physical structural properties of the Herreschoff roaster include 12 hearths with, in total, 45 meters in height and 8 meters in diameter. The operating phenomena of the nickel laterite ore remains similar to the above. The reported total transit time of the roaster is approximately three hours. A simplified overview of the roaster configuration is illustrated in Figure 10, where each of the lower hearths has a pair of burners (12 in total) in which heavy fuel oil is burned under sub-stoichiometric conditions. This generates an atmosphere rich in carbon monoxide which, together with temperatures in the range 600 to 800 degrees Centigrade, causes the reduction of the oxide ore to metalized form.

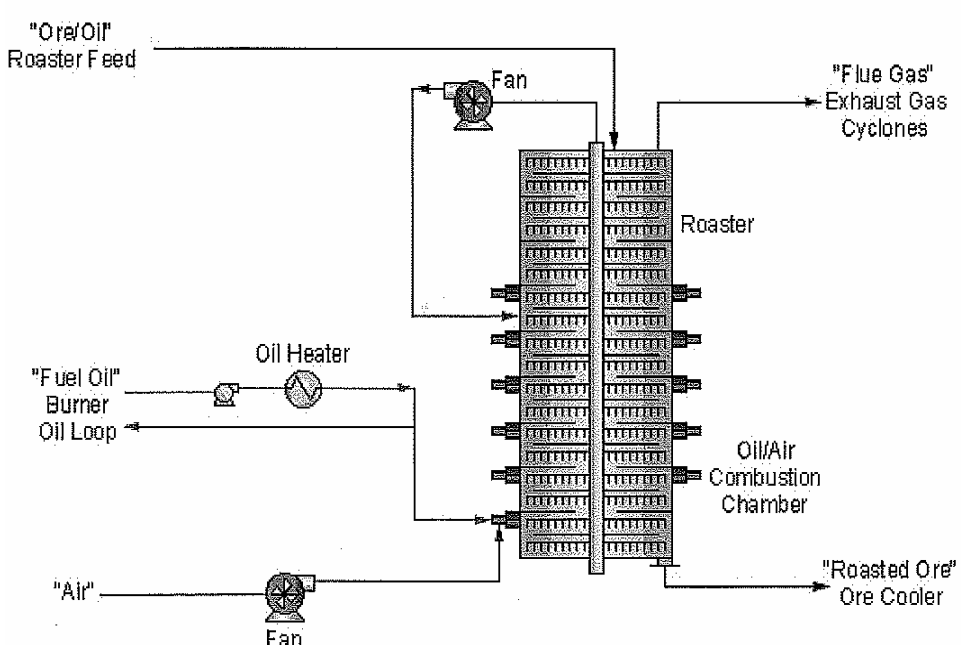

Figure 10 Roaster process overview [30]

The main control objectives are to improve the stability of roaster temperatures, to reduce fuel oil consumption per ton of feed and to increase nickel metallization levels in the roaster product stream. Indeed, the regulation of a hearth temperature is achieved by adjustment of the firing rate (oil flow) of the associated burner. However, each hearth temperature is also strongly affected by the firing rate of the adjacent burners, by the ore feed rate and the secondary air flow. For the optimal metallization of the ore, attainment of the correct temperature profile from top to bottom of the roaster is critical. The target profile is defined as a series of ranges expressing the minimum and maximum acceptable temperatures at each hearth.

The basic automation of the VMN roasters is provided by a network of Allen-Bradley PLCs, with a supervisory SCADA layer implemented by Wonderware InTouch software. For implementing the control algorithms, the Connoisseur software package from Invensys Process Systems was used. The predictive model used in the Connoisseur multi-variable controller has a straightforward

linear time-series format. The model parameters were estimated using response data generated from Pseudo-Random Binary Sequence (PRBS) testing of the roasters. The data allow identifying a high quality multi-variable dynamic model. In order to achieve the control in real-time, the dynamic process model is deployed within a constrained model-predictive control structure, where the control moves are calculated such that the value of a quadratic cost function is minimized subject to linear inequality constraints (QP). The cost function is composed of the following variables: square of the predicted controlled variables (CV) errors over the prediction horizon, square of the incremental manipulated variables (MV) moves over the control horizon and square of the predicted MV deviations from target over the control horizon. The results reported in [45] confirms the superiority of the QP controller as stabilizing comparing a period under Connoisseur control with a similar period under conventional control.

EXPERIMENTAL PART

5 Aim of the experimental part

The main purpose of the MHF control system is to ensure uniform product quality, whereas maximizing the furnace capacity and improving its energy efficiency is necessary for optimal operation. As there is no online product quality and solid temperature measurements available, the process control have to rely on a monitoring technique to improve the control of the calcination progress. In this thesis, a first principal model previously developed in [37] is employed to obtain an estimation of the product composition, and a model-based method (MPC) is selected to design the supervisory control of the furnace. Furthermore, the economic modification of the MPC technique called EMPC is taken in use to incorporate the process economics to control the furnace.

The mechanistic model employed in the thesis is symmetric in the sense that the conditions in each Hearth are assumed to be dependent only on the distance from the hearth center. In contrast, four burners are installed in each of Hearths 4 and 6, providing energy to four quarters of the Hearths independently. In practice, the amount of the energy supplied to every quarter and the temperature measured in different quarters can significantly differ, which makes impossible to use the symmetric first principal model for monitoring and control. Thus, the prerequisite problem is to achieve similar conditions in different sectors of Hearths 4 and 6, which can be solved at the basic level of the control strategy.

The purpose of the experimental part is to setup the simulation environment that prepares the ground for MHF advanced process control development based on EMPC and/or MPC techniques. This includes the revision of the mechanistic MHF model to include more accurate walls dynamics, simplification of the mechanistic model to the state space form suitable for MPC implementation and the design of the basic controllers for Hearth 4 temperature.

The mechanistic model developed in [46] relies on an approximated dynamics of the wall temperature, considering only the temperature of the inner surface and the temperatures between each of the wall material layers. In order to accurately describe the walls temperature dynamics, a detailed model of the heat transfer in the walls have been developed. This wall model describes the dynamics pertaining to the heat transfer flux across the differen in this thesis and incorporated to the mechanistic model.

The implementation of the EMPC requires to simplify a previously developed mechanistic model of the Multiple Hearth Furnace. The simplified model is developed in the form of a nonlinear Hammerstein-Wiener model, which is linearized at every sampling time to carry out the state estimation and MPC optimization tasks. As the accuracy of the simplified process model is crucial for the performance of the EMPC, the thesis aims to compare the simulation results of the mechanistic model and the simplified one.

The EMPC designed in the thesis provides setpoints for the temperature in Hearths 4 and 6, which have to be tightly tracked by the controllers to achieve similar conditions in each quarter of the hearths. The existing temperature control in Hearth 6 performs well, however, the control of Hearth 4 temperature needs to be improved. The experimental part suggests a few alternative controls for the Hearth 4 temperature and presents the simulation results to evaluate the performance of the existing and the proposed solutions.

The experimental part is organized as follows. The MHF is described in Chapter 6. The design of the Economic Model Predictive control for the Multiple Hearth Furnace is provided in Chapter 7. The details of the simulation environment for EMPC implementation are presented in Chapter 8. The comparison of the models and the simulation results are reported in Chapter 9. The current temperature

control in the Hearth 4 is analyzed and the suggested alternative controls are provided and evaluated in Chapter 10. The conclusions are given in Chapter 11.

6 Process Description

6.1 Description of the Multiple Hearth Furnace

This section presents the key physical-chemical phenomena taking place in the solid and the gas phases in the calciner. The Multiple Hearth Furnace (MHF) considered in this Master's thesis is the Herreschoff calciner. The Herreschoff calciner is a furnace with eight chambers called hearths and numbered H1, H2, H3… H8. The furnace has installed four burners to each of the hearths 4 and 6, which supply the heat needed for calcination. The burners are placed with a tangential alignment and have the potential to use a maximum of 8000 kW of power. Raw kaolin is introduced at the top and the temperature increases as it travels down through the furnace.

Within the calciner, the material is moved through the furnaces by the metal plates or blades attached to the rotating rabble arms. The blades are designed with the intention of transporting the material outwards on even-numbered hearths and inwards on odd-numbered hearths. The kaolin traversing the even numbered hearths moves outward to descend through individual holes at the outside border of the hearth, while kaolin moving on the odd-numbered hearths falls to the next hearth through a single annulus located around the shaft supporting the rabble arms at the center. *Figure 11* illustrates the design of the Herreschoff calciner.

An important mechanism of heat transfer inside the furnace is radiation from the flames. This radiation is also reflected by the internal walls of the hearths. As additional mechanisms, conduction and convection heat from the gas phase is transferred through walls and air respectively.

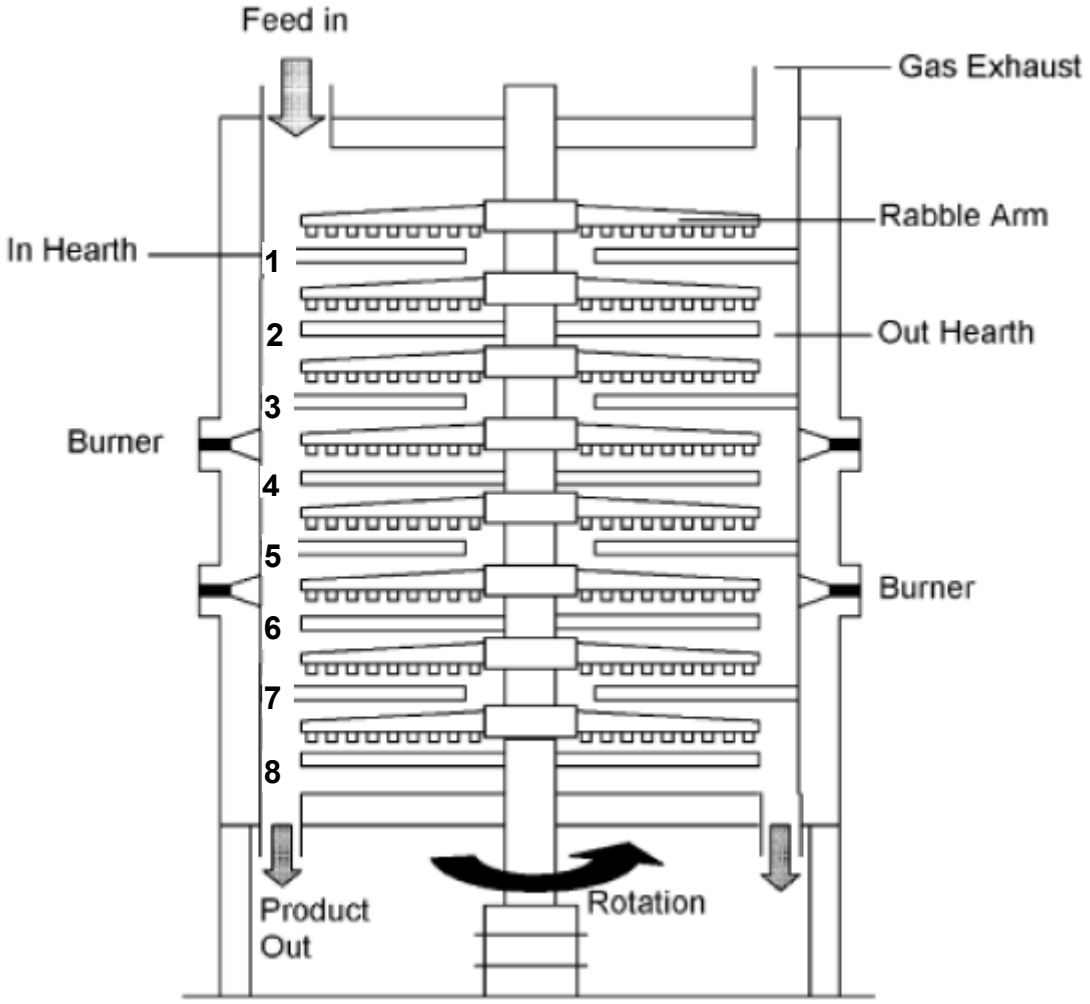

Figure 11. Cross-sectional picture of the Herreschoff calciner with direct fire burners *[32]*

Kaolinite transforms to metakaolin in the hearths 3, 4 and 5. This transformation occurs between 400-700 °C within the furnace. The metakaolin is released from the hearth 5 at a temperature approximately 800 °C which continues to elevate in the hearth 6 where the transformation of metakaolin to the Al–Si spinel phase occurs. The main objective of the hearth 6 is to increase the temperature in order to facilitate the absorption of aluminum into the silica phase. The control of temperature in the hearth 6 is essential to avoid overheating which may result in the undesired formation of a more crystalline material that may generate some

abrasion problems. The reacted material begins to decrease temperature in the hearths 7 and 8 and finally leaves from the hearth 8 at a temperature of 750 °C.

6.2 Overall control scheme of the MHF

The temperature levels in the hearths 4 and 6 are controlled by adjusting the gas flows to the burners. The temperature controllers connected to the burners, maintain the temperatures within the safety limits. Gas and air flow measurements are performed utilizing orifice plate flow meters. Feed rate determines the maximum gas flow allowed in the hearth 4, this limitation prevents an unnecessary use of gas. To ensure a complete combustion of the gas, sufficient amount of air is required, which is controlled by a separate PI controllers. The set-point for combustion air flow is determined according to the stoichiometric ratio between the oxygen and methane in the combustion reaction.

Table 4. Major online measurements and online lab analysis *(provided by IMERYS).*

Measurements	Lab analysis
Hearth 2-8 Mean gas temp. (°C)	Fe_2O_3 (feed)
Feed rate (kg/min)	K_2O (feed)
Mean Gas flow to H4&H6 (m^3/h)	brightness (feed)
Mean Air flow to H4&H6 (m^3/h)	particle size (feed, product)
Kiln exhaust temp. (°C)	Sol. Al. (product)
Kiln rabble arm amps	brightness (product)
Kiln offtake pressure (mBar)	
Gas temp. (°C)	
Combustion air temp. (°C)	

The operating control strategy for the MHF is aimed to process kaolin and calcine it. After setting up the production objectives, the chemical composition of the kaolin is analyzed in earlier process units so that the MHF calciner can be operated on some particular conditions. This analysis including checking the iron

content, mica, feldspar, silica and quartz in the feed to be further processed at higher temperatures in the calciner. The major online measurements and lab data are summarized in Table 4.

The brightness of the product is primarily affected by the temperature profile of the solid material in the furnace. The temperature profile depends on the following variables: the gas temperature of the burners located at the hearths 4 and 6, the shaft rotational speed of the rabble arms and inherently, the feed rate to the calciner. The operators provide the set-points for the target temperature values of the burners in the hearths 4 and 6 separately. The temperature (for each burner) is then adjusted accordingly in a ramp fashion (i.e., the temperature is increased or decreased in a constant rate). The rate in which the temperature is adjusted, is also determined by the operators. Ramp rate allows the temperature to vary either up or down at a rate such that the fabric of the calciner has protection from excessive temperature changes. Control of ramp rate also gives a degree of control to prevent overshoot. The above uses the existing “stand alone" Eurotherm adaptive controllers, where the control is facilitated by modulation of the gas flow. Furthermore, the limits of the gas flow are controlled as well. This prevents temperature overshoot and reduces the consumption of gas, thereby maximizes the energy efficiency of the furnace.

There is an additional requirement of the percentage of soluble aluminum together with brightness specifications, which is checked and taken care by the control strategy. The above discussed control strategy provides a stable control of the kiln.

6.3 A case study of the temperature profile variations

This section aims to demonstrate the effect of disturbances in the MHF on the temperature profile in the furnace while the Hearth 4 and 6 temperature controllers are performing well. The goal of this example is to motivate the need of a supervisory control minimizing the final product quality variations through manipulating the setpoints of the basic temperature controllers.

The case study considers a period of time when the furnace was operated with a feed rate of 100 kg/min. During the considered period, the temperature in the Hearth 6 is tightly controlled, whereas the amount of methane required by this hearth rapidly rises after sample 500 while the temperature in the Hearth 8 drops simultaneously, as it can be seen in Figure 12. In fact, the temperature in Hearth 8 strongly correlates with the temperature of the solids leaving the furnace. Furthermore, the observed drop of the gas and solids temperature in the Hearth 8 is probably caused by lower temperature of the solids leaving from the Hearth 6. At the same time, the methane inflow to the Hearth 4 drops, while the

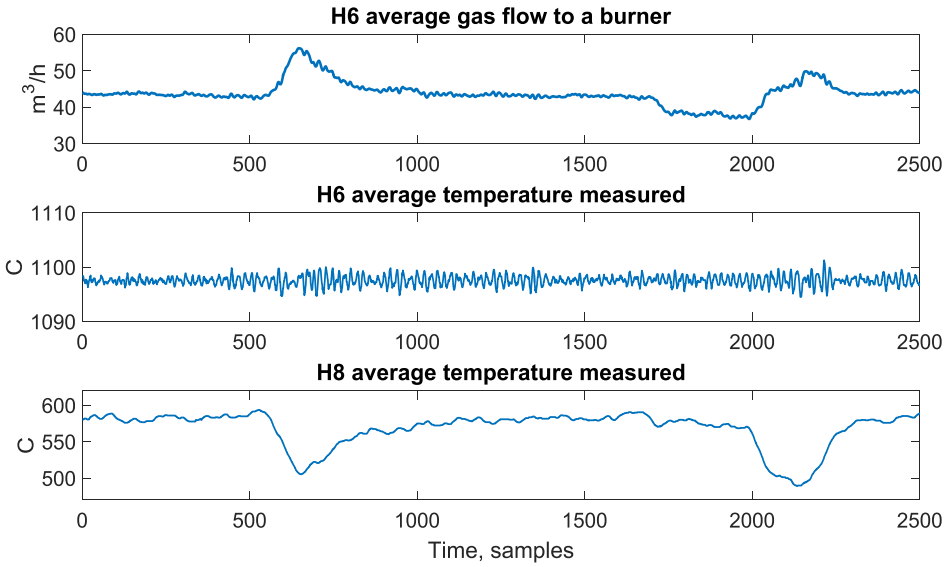

Figure 12. Process variables related to Hearths 6 and 8

temperature in this hearth is stable and the temperature in the Hearth 5 is even increasing, see *Figure 13*.

The observed process variable trends could be explained by partly shifting the exothermic reaction from the Hearth 6 to earlier hearts. This leads to the increase of the temperature in the Hearth 4, which is mostly compensated by the lowered gas flow to the hearth, and also in the Hearth 5. At the same time, less spinel phase is formed in the Hearth 6 causing simultaneous drop of the solid peak temperature reached in this hearth. The effect on the gas temperature in the hearth is fully compensated by the increased methane inflow, but the solid and gas temperature in the subsequent hearths drops. Better understanding of the described phenomena requires more accurate modeling of the heat exchange between the solids and the gas phase, especially in the Hearths 4 to 6.

The provided case study confirms that tracking the temperature in the Hearths 4 and 6 is not able to eliminate variations of the temperature profile in the furnace

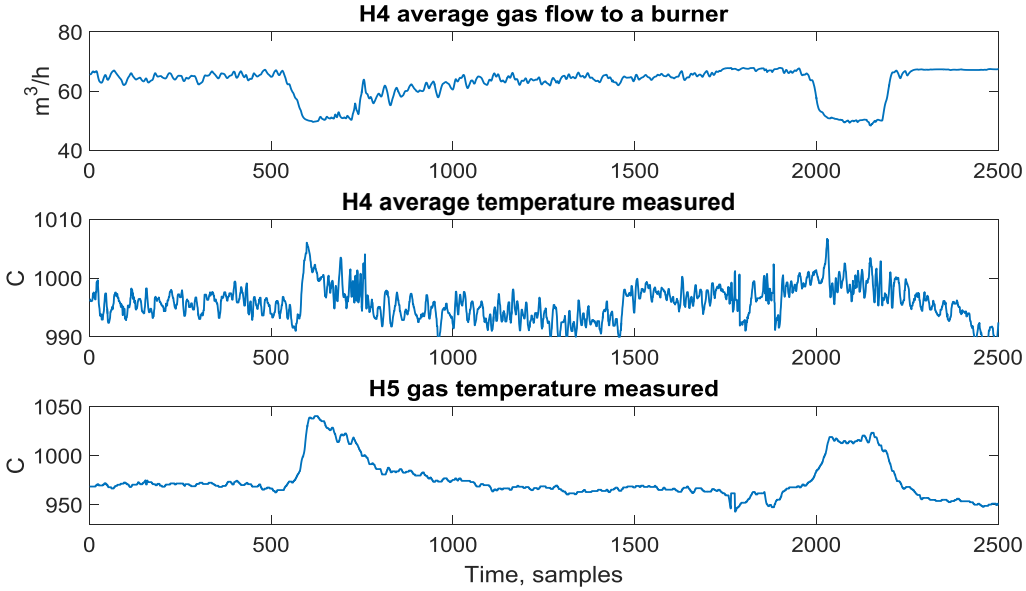

Figure 13. The process variables related to the Hearths 4 and 5

completely. In fact, many similar cases are found in the process data, especially for the high feed rates.

7 Design of Economic MPC for the Multiple Hearth Furnace

This chapter describes the design of EMPC for the MHF. The overall control strategy based on the EMPC is given in Section 7.1 and the rest of the section describes the elements of the EMPC. In more details, the cost function is explained in Section 7.2 and the process models are introduced in Section 7.3.

7.1 EMPC control strategy

The EMPC control designed in the thesis aims to optimize the temperature profile in the furnace through determining the feed rate and providing the setpoints to the basic temperature controllers in the Hearths 4 and 6, as shown in *Figure 14*. Assuming the basic temperature controllers are operating properly, the temperature measured in the Hearths 4 and 6 is close to the setpoints provided by the EMPC. Thus, the main feedback from the process to the controller is the gas consumption in the Hearths 4 and 6 and the gas temperature measured in other hearths. In addition, the updated prices of calcined kaolin and methane are used to calculate the objective of the EMPC optimization. The constraints have to be also specified to maintain proper operating conditions and prevent damage to the furnace.

The EMPC relies on a process model to predict and optimize the future plant behavior in on-line. As the mechanistic model is too complicated to implement the necessary computations, a simplified model is used for the EMPC development. Furthermore, the simplified model is linearized at each EMPC run resulting in the following model:

$$\begin{cases} x_{t+1} = Ax_t + Bu_t, & t \in \mathbb{I}_{[0,N-1]} \\ y_t = Cx_t + Du_t \end{cases} \tag{59}$$

where x_t is the state of the furnace, y_t contains the temperatures T_{Hi} measured in the Hearth $i = 1, \dots, 8$, u_t contains the feed rate to the furnace F_K and the gas flow rates F_{g4} and F_{g6} to the Hearths 4 and 6 respectively:

$$y_t = \begin{bmatrix} T_{H1} \\ T_{H2} \\ \dots \\ T_{H8} \end{bmatrix}, u_t = \begin{bmatrix} F_K \\ F_{g4} \\ F_{g6} \end{bmatrix}.$$

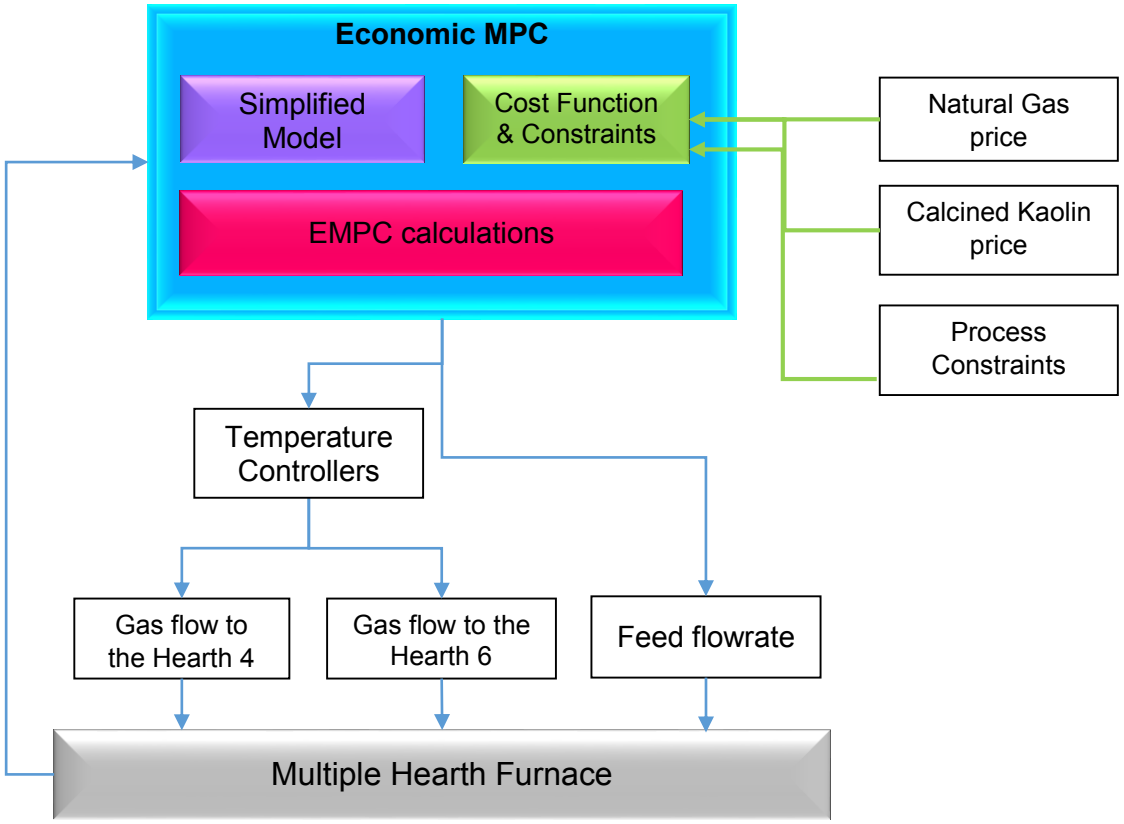

Figure 14. EMPC control strategy for the MHF

Both the mechanistic model and its simplification represent the open loop furnace dynamics, while the EMPC handles the process running in the closed loop with the temperature controllers. In more details, the EMPC manipulates the setpoints for the gas temperatures in the hearths 4 and 6 and considers the gas flows to the hearths as the feedback from the process. In opposite, the mechanistic and the simplified models consider the gas flow rates and the feed flow as the inputs

to predict the temperature profile in the furnace. Thus, the open-loop dynamics (59) has to be converted to the close-loop model to be used in the EMPC calculations.

Assuming the measured temperatures in the Hearths 4 and 6 equal to the setpoints y_t^* provided by the EMPC, the inputs can be expressed from the second equation in (59):

$$u_t = D^{-1}(y_t^* - Cx_t) \tag{60}$$

Substituting the last equation to Equation (59), the closed loop dynamics for the state is derived:

$$x_{t+1} = Ax_t + BD^{-1}(y_t^* - Cx_t) \tag{61}$$

Thus, system of Equations (60), (61) represents the closed loop model that is necessary for EMPC implementation that can be formulated as follows:

$$\begin{gathered} \max_{y_t^*} J_{MHF}(u_t) \\ \begin{cases} x_{t+1} = x_t + BD^{-1}(y_t^* - Cx_t), & t \in \mathbb{I}_{[0,N-1]} \\ u_t = D^{-1}(y_t^* - Cx_t) \end{cases} \\ x_0 = x(0) \\ (x_t, y_t^*) \in \mathbb{Z}, \quad t \in \mathbb{I}_{[0,N-1]} \\ x_N = x(N) \in \mathbb{X}^f \end{gathered} \tag{62}$$

y_t^* contains the setpoints for the Hearths 4 and 6 temperature control. As the EMPC optimization problem is defined, it is possible to provide more details of the design.

7.2 Cost Function

The economic interest of the process is to maximize production of the calcined kaolin and at the same time to minimize energy consumption. The flow rate of the calcined output (F_C), which contains the product of interest, is calculated using simple mass balances of the form:

$$F_C = (1 - c_{H2O}) * (1 - c_{fm}) * F_K \quad (63)$$

From [37], it is known that when the kaolin enters the process, it releases approximately 14% of its weight through evaporation and dehydroxylation (c_{H2O}), as explained in Section 4.2. Additionally, the calcined product contains approximately 0.5% free moisture (c_{fm}) when it leaves the process.

Other interest, as mentioned earlier, is to minimize the energy consumption. In the Multiple hearth furnace, the main energy provider is the methane gas, which is combusted to increase temperature inside, and to reach the desired levels to initiate the different chemical reactions that occur inside the furnace.

The methane entering the process is burned in the hearth 4 and hearth 6, and the variables for gas flow for the H4 and H6 are F_{g4} and F_{g6} respectively. The total gas flow entering the system is defined as:

$$F_g = F_{g4} + F_{g6} \quad (64)$$

To build the cost function it is important to include the price for the variables involving the process economics. In this way, the cost function is expressed as an equation that contains the main economic interest of the process (profit).

$$J_{MHF} = \sum_{t=0}^{N} p_C F_C - p_g F_g \quad (65)$$

Where p_C and p_g are the respective prices of calcined kaolin and methane gas, and J_{MHF} is the Economic Performance Index of the MHF for a specific interval of time [0,N].

7.3 Models for the Multiple Hearth Furnace

This section presents the models used for the EMPC development. In the first subsection, the mechanistic model of the MHF based on physical and chemical principles is presented. In this thesis, the mechanistic model is modified to include detailed walls dynamics presented in the second subsection. Next, the mechanistic model with the detailed walls dynamics is simplified and the resulting model is presented in the third subsection. In the last subsection, the linearization of the simplified model, necessary for the EMPC implementation, is introduced.

7.3.1 Mechanistic model of the MHF

In the work of Eskelinen [46], a mechanistic model of the MHF was developed. In this work, the MHF was divided in six parts: the gas phase, solid bed, central shaft, walls, rabble arms, and the cooling air. In this Section the basic equations used in this model will be presented, for more details please refer to [46].

The MHF considered by Eskelinen, consists of eight hearths and it is designed with a counter-current solid and gas flows as described in Section 6.1. The calcination process requires great amounts of heat, and it is supplied to the furnace through a total of eight methane burners distributed between the Hearths 4 and 6.

Some assumptions have been taken into consideration to develop the model. Primarily, the solid bed on the hearths are split into four (Hearths 3 to 8) or five (Hearths 1 and 2) homogenous annular volumes depending to the furnace rabble arm configuration. As a second consideration, the volumes are assumed to be identical in size in the mass content and the radial direction. In third instance, the mixing model assumes that one shaft rotation disperses the contents of a volume between the original volume and its neighbor volumes (one is the following and

the other is the preceding). Finally the solid mass distribution after one time rotation is defined as:

$$m_{t+1}^{j} = D_j \cdot (m_t^j - R_{r,t}^j) + m_{feed,t}^j \quad (66)$$

Where $m_{feed,t}^j$ and $R_{r,t}^j$ denote the feed to the Hearth and the mass loss in the solid phase in the Hearth j. The mass movement matrix D defines the distribution of the contents of each partition m_t^j after one central shaft rotation in the hearth *j,* specifically, the column i of the matrix represents the distribution of volume i between the volumes of the hearth.

The feed to a hearth may be determined as the exiting volume from the previous hearth as follows:

$$m_{feed,t}^j = \left(1 - \sum D_{j-1}^K\right)\left(m_t^{j-1,K} - R_{r,t}^{j-1,K}\right) \quad (67)$$

Where K is the exiting volume of hearth $j-1$ and D_{j-1}^K is the K[th] column of matrix D_{j-1} . Defining the solid bed movement matrix for the H1 as:

$$D_1 = \begin{bmatrix} 1-a_1 & a_1 & 0 & 0 & 0 \\ a_1-\alpha & 1-2\,a_1+\alpha & a_1 & 0 & 0 \\ 0 & a_1-\alpha & 1-2\,a_1+\alpha & a_1 & 0 \\ 0 & 0 & a_1-\alpha & 1-2\,a_1 & a_1 \\ 0 & 0 & 0 & a_1 & 1-a_1 \end{bmatrix} \quad (68)$$

The parameter α is presented to define the net forward flow through a hearth, this is the feed rate minus the mass loss caused by dehydroxylation reactions and evaporation. a_1 is the upper diagonal matrix elements and represents the flow from the current volume to the next volume. Therefore, the lower diagonal matrix elements $(a_1 - \alpha)$ represents the flow equal to the difference of the full forward and the net forward flows.

The gas phase mass balance equation is determined as:

$$\dot{n}_{i,in} - \dot{n}_{i,out} - R_i = 0 \quad (69)$$

Where $n_{i,out}$ signifies the number of moles of component i leaving a volume, R_i is the mass difference of component i due to reactions, and $n_{i,in}$, represents the incoming moles of component i, obtained as follows:

$$n_{i,in}^{j} = c_i^{j+1} F^j \quad (70)$$

F_j is the gas flow passing through the Hearth, c_i^{j+1} is the concentration of component i in the previous volume, and *j* is the number of the volume.

For each hearth having different temperature, the real volumetric gas flow F_{real}, can be calculated based on the ideal gas law as:

$$F_{real} = F_{NTP} \frac{T_{real}}{T_{NTP}} \quad (71)$$

where F_{NTP} is the volumetric flow calculated from atmospheric temperature and pressure.

The model also takes in consideration energy balances for the walls, gas phase, the central shaft, cooling air, rabble arms, and for the solid bed:

$$\dot{Q}_{gas,in} - \dot{Q}_{gas,out} + \dot{Q}_{combustion} + \dot{Q}_{gs} + \dot{Q}_{gw} + \dot{Q}_{gshaft} + \dot{Q}_{garms} = 0 \quad (72)$$

Where $Q_{gas,in}$ and $Q_{gas,out}$ denote the heat of the inlet and the outlet gas flows, $Q_{combustion}$ is the heat released by the combustion, and the final four terms in the left side of the equation, denote the heat exchange of the gas phase with the solid, walls, central shaft and the arms.

The combustion energy is obtained:

$$\dot{Q}_{combustion} = b_i \dot{n}_{methane} \Delta H_{combust} \quad (73)$$

Where b_i is the combustion ratio, $n_{methane}$ represents the methane feed rate, and $\Delta H_{combust}$ is the combustion enthalpy of methane.

Heat transfer between the solid and gas phase $\dot{Q}_{gs}$ takes place through radiation and convection:

$$\dot{Q}_{gs} = \sigma X_s A_{gs} \varepsilon_s \varepsilon_g (T_g^4 - T_s^4) + h_{cgs} X_s A_{gs} (T_g - T_s) \quad (74)$$

Where A_{gs} is the area of the Hearth floor, σ is the Stefan-Boltzmann constant. Solid and gas emissivities ε_s and ε_g, and heat transfer coefficient h_{cgs}. T_g and T_s are the temperatures of the gas and the solid respectively. X_s is a surface view factor.

Heat transfer among the inner walls and the gas phase $\dot{Q}_{gw}$ takes place by convection and radiation:

$$\dot{Q}_{gw} = \sigma A_{gw} \frac{(\varepsilon_w + 1)}{2} \varepsilon_g (T_g^4 - T_w^4) + h_{cgw} A_{gw} (T_g - T_w) \quad (75)$$

A_{gw} is the area of the walls, ε_w and ε_g is the emissivities of the walls and the gas, T_g and T_w are the temperatures of the gas and the walls respectively, and h_{cgw} is the heat transfer coefficient.

The heat flux between the gas phase and the central shaft $\dot{Q}_{gshaft}$, and between the gas phase and rabble arms $\dot{Q}_{garms}$ comprises the radiative and the convective heat transfer terms respectively:

$$\dot{Q}_{gshaft} = \sigma Z A_{gshaft} \varepsilon_{shaft} \varepsilon_g (T_{gas}^4 - T_{shaft}^4) + h_{cgshaft} Z A_{gshaft} (T_{gas} - T_{shaft}) \quad (76)$$

$$\dot{Q}_{garms} = \sigma A_{garms} \varepsilon_{arms} \varepsilon_g (T_{gas}^4 - T_{arms}^4) + h_{cgarms} A_{garms} (T_{gas} - T_{arms}) \quad (77)$$

Where A_{gshaft} and A_{garms} are the areas of the central shaft and the arms respectively, ε_{shaft}, ε_{arms} and ε_g are the respective emissivities of the shaft, the arms and the gas, while T_{shaft}, T_{arms} and T_g are the temperatures of the model parts respectively, h_{gshaft} and h_{arms} are the heat transfer coefficients, and Z is a constant describing the insulation of the central shaft.

The energy balance equation for the walls is:

$$\frac{\partial Q_w}{\partial t} = \dot{Q}_{wg} - \dot{Q}_{ws} - \dot{Q}_{wa} \quad (78)$$

Q_w is the heat accumulated in the walls, and $\dot{Q}_{wg}$ and $\dot{Q}_{wa}$ symbolize the heat transfer between the walls and the gas, and the walls and the ambient air.

The radiative heat flux is obtained as:

$$\dot{Q}_{ws} = \sigma X_s A_{sw} \varepsilon_{sw} \, (T_w^4 - T_s^4) \tag{79}$$

X_s and A_{sw} are the form factor of the solid surface and the area of the Hearth floor, and the emissivity between the solid bed and the walls is symbolized ε_{sw}.

The following equation is used to obtain the heat transfer between the outer wall and the ambient air:

$$\dot{Q}_{wa} = h_{cwa} A_{wa} (T_{ambient} - T_{outer\,wall}) \tag{80}$$

A_{wa} is the surface of the outer layer of the furnace wall, $T_{ambient}$ and $T_{outer\,wall}$ are the respective temperatures of the ambient air and the outer layer of the wall, finally h_{cwa} is the heat transfer coefficient. With the purpose of calculating temperature profile, the furnace wall is divided into eight segments according to the hearths distribution.

The equations describing the heat in the central shaft and the rabble arms are respectively:

$$\frac{\partial Q_{shaft}}{\partial t} = \dot{Q}_{gshaft} - \dot{Q}_{shaft,cool} \tag{81}$$

$$\frac{\partial Q_{arms}}{\partial t} = \dot{Q}_{garms} - \dot{Q}_{arms,cool} \tag{82}$$

Where the heat exchange among the gas and shaft, gas and arms, respectively are denoted by Q_{gshaft} and Q_{garms}.

The heat transfer between cooling air and the central shaft and the rabble arms correspondingly are obtained:

$$\dot{Q}_{shaft\_cool} = \sigma A_{shaft\_cool} \varepsilon_{shaft} \;\; (T_{shaft}^4 - T_{cool}^4) + h_{cshaft\_cool} A_{shaft\_cool} (T_{shaft} - T_{cool}) \tag{83}$$

$$\dot{Q}_{arms\_cool} = \sigma A_{arms\_cool}\varepsilon_{arms}(T_{arms}^4 - T_{cool}^4) + h_{carms\_cool}A_{carms\_cool}(T_{arms} - T_{cool}) \quad (84)$$

A_{shaft_cool} and A_{arms_cool} are the surfaces of the central shaft and the arms, $\varepsilon_{shaft}$and ε_{arms} are the emissivities of the shaft and the arms, while T_{shaft}, T_{arms} and T_{cool} are the temperatures of the model parts respectively, h_{cshaft_cool} and h_{carms_cool} are the heat transfer coefficients.

The energy balance of the cooling air:

$$\frac{\partial Q_{cooling\ air}}{\partial t} = \dot{Q}_{cooling\ air,in} + \dot{Q}_{arms,cool} + \dot{Q}_{shaft,cool} - \dot{Q}_{cooling\ air,out} \quad (85)$$

Where $\dot{Q}_{coolingair,in}$ and $\dot{Q}_{coolingair,out}$ are the heat of the inlet and outlet cooling, while $\dot{Q}_{shaft,cool}$ and $\dot{Q}_{arms,cool}$ symbolize the respective heat exchange concerning the cooling area and the central shaft and the arms.

Finally, the solid phase energy balance equation is obtained:

$$\frac{\partial Q}{\partial t} = \dot{Q}_{mass,in} - \dot{Q}_{mass,out} - \dot{Q}_{reactions} - \dot{Q}_{evaporation} + \dot{Q}_{sw} + \dot{Q}_{sg} \quad (86)$$

Where Q denotes the solid phase heat of a volume, $\dot{Q}_{mass,in}$ and $\dot{Q}_{mass,out}$ denote the solid phase heat, inflowing and outflowing the volume, $\dot{Q}_{reactions}$ and $\dot{Q}_{evaporation}$ define the heat of the chemical reactions occurring in the solid phase and free water evaporation, while the final two terms symbolize the heat exchange concerning the solid bed and the walls, and the solid bed and the gas.

The heat in each solid bed partition can be obtained in a similar manner as previously defined in Equation (63):

$$Q_{t+1}^{j,k} = D_j \cdot Q_t^{j,k} + Q_{feed,t} \quad (87)$$

7.3.2 Detailed model of the furnace wall

This section discusses the role of the walls in the heat transfer routes in the furnace, which is followed by the description of the detailed model of the walls dynamics. In more details, the furnace walls are involved in the following heat transfer routes: the walls transfer the energy obtained from the gas phase to the solids, the walls accumulate thermal energy and the walls conduct heat from the furnace to the ambient causing energy losses [47]. The first route, which is the energy transfer from the walls to the solids through radiation, is known to be very significant. A calculation from the mechanistic model shows that a variation of 10K in the temperature of the inner walls in the Hearth 6 affects the heat transfer to the solid by 100 kW, and this is noticeable in the process scale.

In order to estimate the effect of the heat accumulation in the walls on the energy fluxes in the furnace, the walls heat capacity has been calculated based on the material properties provided in *Table 5*. The estimated heat capacity of the walls is around 80 MJ/K, which means that only minor energy fluxes are generated by accumulating/releasing heat by the walls due to very slow dynamics of the walls temperature. As an example, rising the walls temperature by 10 °C during 24 hours would only require approximately 9 kW of heating power, which is negligible in the process scale. Next, the total heat losses, estimated based on the material properties provided in *Table 5*, are about 90 kW, which is around 2% of the energy released from methane combustion in the furnace. Thus, the heat losses represent a minor component of the energy balance of the process, and the variations in the heat losses have negligible effect on the furnace dynamics. In brief, it can be concluded that the temperature of the inner walls has a strong influence on the intensity of the radiation emitted by the wall surface, whereas the heat accumulation in the walls can be neglected and the heat losses can be assumed constant.

Table 5. Material properties (provided by Imerys)

Material	Width	Conductivity (W/m K)	Heat capacity (J/Kg K)	Density (Kg/m^3)
Refractory	152	1.6	1000	2480
Fire bricks	114	0.32	1000	769
Backfill	75	0.16	1000	2350
Steel	25	54	465	7833

The mechanistic model developed in [46] relies on an approximated dynamics of the wall temperature, considering the temperature of the inner walls and the temperature between the material layers shown in *Table 5*. In order to accurately describe the dynamics of the inner walls temperature, a detailed model of the heat transfer in the walls have been developed in this thesis. The walls are divided into 5 mm thick layers, whereas the first and the last layers represents the outer and the inner wall respectively, and the total number of layers is denoted as N. The temperature T_i of each layer $i = 1, \dots, N$ is assumed to be uniform. The implicit finite difference approximation of the temperature dynamics of layer i is as follows:

$$\frac{(T_{t+1}^i - T_t^i)Cp_i}{\Delta t} = \frac{(T_t^{i-1} - T_t^i)k_i}{2d} + \frac{(T_{t+1}^{i-1} - T_{t+1}^i)k_i}{2d} + \frac{(T_t^{i+1} - T_t^i)k_i}{2d} + \frac{(T_{t+1}^{i+1} - T_{t+1}^i)k_i}{2d} \quad (88)$$

where t denotes the time step, Cp_i and k_i are the heat capacity and the heat conduction coefficient of volume i, computed according to the material properties taken from *Table 5*, and d= 5mm is the spatial step.

The heat inflow through the inner surface (Q_t) of the walls is assumed to be linearly depend on the inner wall temperature, where Δ is the linear part coefficient:

$$Q_t = Q^* + \Delta\, T_t^N \quad (89)$$

and the temperature of the inner wall layer is approximated as follows:

$$\frac{(T_{t+1}^N - T_t^N)Cp_i}{\Delta t} = \frac{(T_t^{N-1} - T_t^N)k_N}{2d} + \frac{(T_{t+1}^{N-1} - T_{t+1}^N)k_N}{2d} + Q_t \quad (90)$$

Starting from the initial temperature of the walls $T_0^i, i = 1, \dots, N$, the algorithm resolves the system of equations (88), (90) at every time step t to obtain the temperature profile within the walls at the next instant $t + 1$.

In order to study the dynamics of the inner walls temperature, the coefficient Q^* describing the heat inflow to the walls was varied and the resulting steady state temperature of the inner walls is presented in *Figure 15*. The linear part coefficient Δ was assumed to be $\Delta = 0.17\mathrm{kW/m^2}/K$ in (92), which roughly represents the conditions in the Hearth 6.

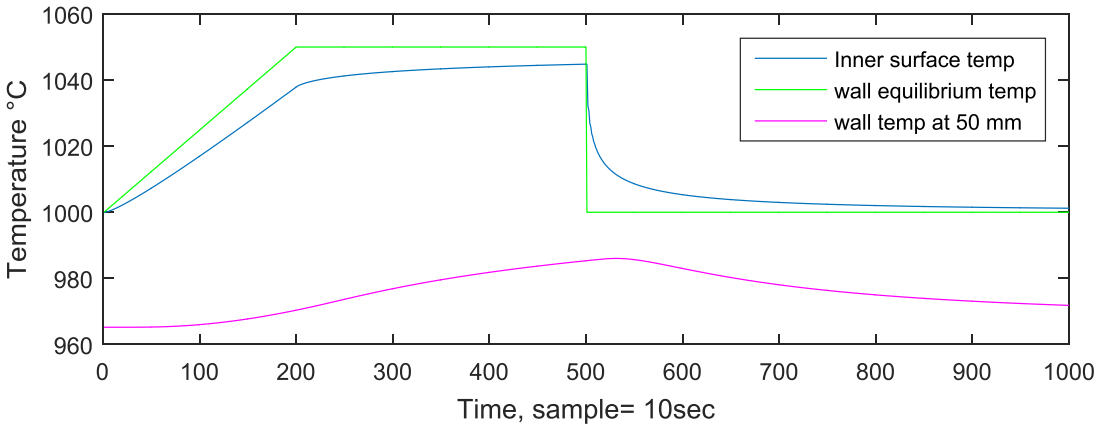

Figure 15. Simulation results of the detailed walls temperature model

In general, the inner walls temperature follows its steady state with a short delay, which can be described by a dynamics with the settling time less than 1 hour. Compared to the inner surface, the inside of the wall shows considerably slower dynamics, with the settling time of more than a day. In fact, the temperature inside the walls have a minor effect on the inner surface temperature, causing it to approach the steady value very slowly between samples 200 and 500, as shown in *Figure 15*.

Based on this comparison, it is possible to conclude that the temperature of the inner wall is important due to its effect on the radiative energy transference inside the furnace, which provides heat to the solid. The main component of the inner walls temperature dynamics has a settling time below 1 hour, whereas the slow temperature dynamics inside the walls has a minor effect on the inner surface.

7.3.3 Simplified model

For the purpose of future implementation of a nonlinear model to MPC or EMPC, a simplified model based on the mechanistic model described in Section 7.3.1 has to be developed. A simplification of the mechanistic model is built based on its dynamics and nonlinear behavior separately. By separating the behavior in a nonlinear static block and a linear dynamic block, it is possible to construct a model that retains the response of the original. For the case where the linear dynamic block is preceded by a static input nonlinearity the model is known as a Hammerstein model and for the alternative case where the linear dynamic block is followed by a static nonlinearity, the model is identified as a Wiener model [48].

The simplified model is expressed as a Hammerstein-Wiener model (HWM). The HWM separates the dynamic system in blocks that contain the nonlinearities in static form and the dynamics in linear form. The linear block, which encloses the dynamics of the process, is preceded and followed by a static non-linear block.

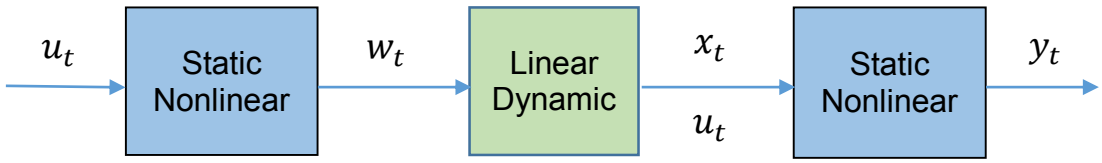

Figure 16. Structure of Hammerstein-Wiener model *[33]*

Figure 16 shows the structure of the HWM which denotes the dynamic process by means of input and output static nonlinear blocks in between dynamic linear blocks which is affected by static nonlinearities. The Hammerstein-Wiener structure is then utilized to capture the physical nonlinear effects in the process that will influence the input and output of the linear system.

As discussed in the previous section and in [46], the dynamics of the MHF includes the very fast component, relating to the gas phase, and the slower component, representing the solid state. For EMPC implementation the

temperature of the solid has to be described dynamically. Furthermore, as the temperature of the inner layer of the walls has a direct effect on the calcination process happening in the furnace, it is also considered in the model as a state. The gas temperature profile could be modeled with algebraic equations. Additionally the spinel phase content and/or mullite content may be included as an output in order to control the quality of the product.

The simplified model is implemented as the following Hammerstein-Wiener nonlinear dynamic model:

$$\begin{aligned} x_{t+1} &= \alpha x_t + (1-\alpha)F(u_t) \\ y_t &= G(u_t, x_t) \end{aligned} \qquad (91)$$

Where u_t are inputs to the process (kaolin feed, gas flows to the H4 and H6), x_t contains the temperature of the solids in each volume of the furnace and the internal wall temperature in the hearths, α is a parameter characteristic of the HWM and is obtained through identification using the identification toolbox included in the numerical computing environment MATLAB®. $F(u_t)$ and $G(u_t, x_t)$ are static nonlinear functions obtained from the mechanistic model simulations and energy balances respectively.

In order to implement the first function $F(u_t)$, describing the steady-state values of the process, a look up table has been created by running the mechanistic model simulations with different process inputs. The obtained values are interpolated as follows:

$$F(u_t) = \sum_{i=1}^{5}\sum_{j=1}^{5}\sum_{k=1}^{5} b_{i,j,k}\, h_i^x(F_K) h_j^y\left(F_{g4}\right) h_k^z\left(F_{g6}\right) \qquad (92)$$

where $b_{i,j,k}$ are the values from the look-up table and the piecewise linear basis functions h_i^x, h_j^y and h_k^z have been used for the interpolation, as shown in *Figure 17*:

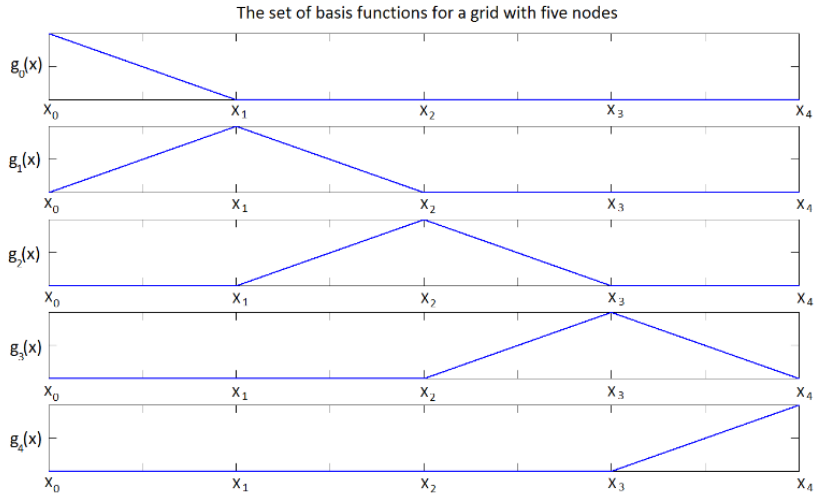

Figure 17. The basis function used for the interpolation in Equation *(92)*

The second function $G(u_t, x_t)$, describing the steady state values of the gas temperature next to the walls in the Hearths (the temperature profile), is implemented by resolving the energy balance for the gas phase derived from the mechanistic model.

7.3.4 Linearization of the simplified model

The mechanistic model includes a large number of nonlinear differential and algebraic equations, and therefore, it is unsuitable for model predictive control implementation. The simplified model developed in this work, is aiming to limit the number of states of the model and to achieve a simple equations structure, thus, making the simplified model suitable for the online optimization. Furthermore, the simplified model contains the energy balance of the furnace as algebraic equations in order to utilize the physical-chemical knowledge collected in the mechanistic model. To implement the simplified model for the EMPC structure a further step should be made. A linearization of the HWM for the furnace is performed online in order to reduce the complexity and number of calculations.

The simplified model in Equation (91) is linearized by approximating the nonlinear terms in the right hand of the equations by linear functions. In particular, the first function $F(u_t)$ has been approximated with a truncated Taylor series to the first term for each variable as follows:

$$F(u_t) \approx F^0({F_K}^*, {F_{g4}}^*, {F_{g6}}^*) + \frac{\partial F}{\partial F_K}(F_K - {F_K}^*) + \frac{\partial F}{\partial F_{g4}}(F_{g4} - {F_{g4}}^*) + \frac{\partial F}{\partial F_{g6}}(F_{g6} - {F_{g6}}^*) \quad (93)$$

where the derivatives in the right side part in Equation (93) are calculated, therefore differentiating analytically the function $F(u_t)$ that is defined according to Equation (92). After approximating to a Taylor series the function $F(u_t)$ may be expressed as part of a linear state space model:

$$F(u_t) \approx Bu_t + F^0({u_t}^*) \quad (94)$$

The dynamic part in this model remains the same as the HWM, because it is linear in nature, consequently the matrix A is an identity matrix with a congruent size.

For the linearization of the second function $G(u_t, x_t)$, a simple unity step up and down response was used to determine the linear terms that constitute the state space model. Therefore the function is to be reduced to the following form:

$$G(u_t, x_t) \approx Cx_t + Du_t + G^0({u_t}^*, {x_t}^*) \quad (95)$$

To determine the values of C and D a numerical derivative approximation is applied, as a unitary increase and decrease to the state variables and process inputs respectively, while G^0 is only a constant associated to the initial value, analogous to $F^0({u_t}^*)$. Thus these matrices are obtained according to:

$$C = \frac{G(u_t, x_t + \Delta_x) - G(u_t, x_t - \Delta_x)}{2\Delta_x}$$
$$D = \frac{G(u_t + \Delta_u, x_t) - G(u_t - \Delta_u, x_t)}{2\Delta_u} \quad (96)$$

Where Δ_x and Δ_u are vectors constituted of unitary values corresponding to each of the states and process variables respectively. Finally the linearization model may be expressed according to the following system:

$$\begin{aligned} x_{t+1} &= \alpha A x_t + (1-\alpha)[Bu_t + F^0(u_t{}^*)] \\ y_t &= Cx_t + Du_t + G^0(u_t{}^*, x_t{}^*) \end{aligned} \tag{97}$$

As it is noticeable, the system in Equation (97) is expressed as a linear state space model. This model is suitable for EMPC implementation as demonstrated in Section 2.2.1, because it facilitates the prediction of states, which is the fundamental basis of Predictive Control strategies.

8 Setup of the MHF simulation environment for advanced process control implementation

This chapter describes the simulation environment created in this thesis for implementation and testing of advanced process controls of the MHF, like the EMPC designed in the previous section. In particular, the overview of the simulation environment is provided and the details of the EMPC implementation are discussed.

The simulation environment developed in this work is implemented in MathWorks™ MATLAB®. This software includes a fourth generation programming language, which handles matrix calculations, implementation of algorithms, interfacing with other programs, plotting of diverse data, among others. MATLAB is broadly used in research and academic institutions, as well as in industry, due to the ease of access, fast processing and reliability.

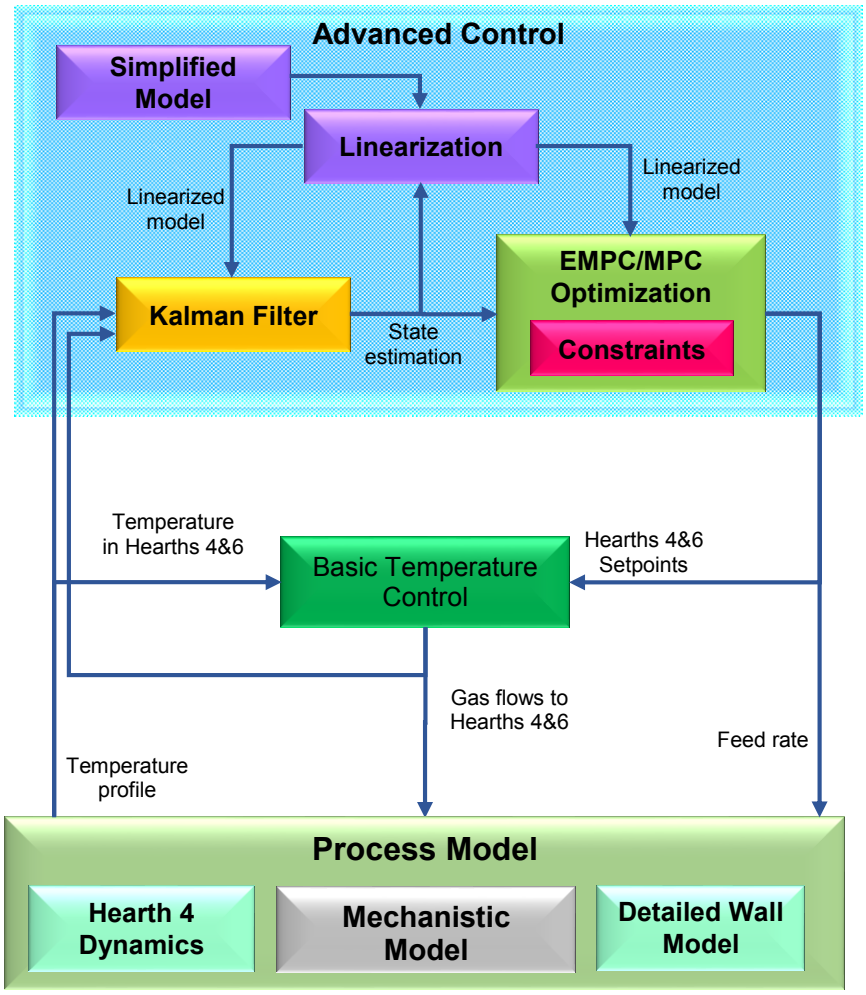

Figure 18. Simulation environment for advanced process control development

The overview of the simulation environment is shown in *Figure 18* above. The mechanistic model including the detailed walls dynamics is used to simulate the actual process behavior. The model obtains the gas flow rates to Hearths 4 and 6 from the basic temperature PI controllers and the feed rate from the advanced controller optimization. The temperature profile predicted by the model and the gas flow rates to Hearths 4 and 6 are supplied to the Kalman filter estimating the current state of the furnace. The simplified model is linearized at the estimated state, and the linear model is utilized in the MPC/EMPC optimization. In addition,

the Kalman filter receives the linear model to carry out the state estimation at the next time step.

In order to carry out simulation studies, some variables should be defined, including the calcined Kaolin price and the methane gas price. Within each EMPC optimization, the prices are assumed to be constant equal to the current price values, whereas the gas and product prices can vary during simulations.

The necessary parameters for the first principle model are obtained from [37]. The simulator designed in the work of Eskelinen [37] enhanced to include the detailed walls dynamics and the dynamics of Hearth 4 temperature is employed as the process of interest, in this case the Herreschoff calciner. This simulator takes in consideration the equations described Section 7.3.1 to model in its entirety the MHF, and was implemented likewise in MATLAB.

The optimization problem is solved, by predicting the states using the linearized model and calculating the optimal temperature setpoints, through the solution of the optimization problem in Equation (98):

$$
\begin{aligned}
&\max_{y_t^*} \sum_{t=0}^{N} p_C F_C - p_g F_g \\
&\begin{cases} x_{t+1} = \alpha A x_t + (1-\alpha) B D^{-1}(y_t^* - C x_t) \\ u_t = C x_t + D u_t \end{cases} \quad t \in \mathbb{I}_{[0,N-1]} \\
&F_K \in [95, 115]\ Kg/min \\
&F_g/F_K \in [2.96, 3.12] mol/kg \\
&F_{g4}/F_g \in [0.56, 0.63] \\
&T_{H4} \in [980, 1020]\ °C \\
&T_{H6} \in [1068, 1108]\ °C \\
&\Delta F_K \in [-5, 5]\ Kg/min \\
&\Delta F_{g4}, \Delta F_{g6} \in [-5, 5]\ m^3/h
\end{aligned}
\tag{98}
$$

where p_C and p_g denote the calcined kaolin and methane prices respectively. The equations above include all process constraints, the linearized model and the cost functions described in Chapter 7. In more details, the first equation in (86) represents the economic objective to be maximized. The second and the third equations represent the closed loop dynamics of the simplified model governed by the basic temperature controllers. The matrixes A, B, C and D and the time constant α are obtained from the linearized model (97) and converted to the closed loop model according to the system of Equations (60), (61). Equations four to six in (98) represent the constraints on the feed rate, the specific energy provided to the furnace and the combustion gas distribution between the Hearths. These limits have been estimated from the process data. Equations seven and eight in (98) impose the limits on the gas temperature in the Hearths 4 and 6 in order to restrict the operating conditions to the commonly used. The last two equations in (98) prevent rapid variations of the combustion gas flows to the furnace in order to avoid wall material damage.

After solving the optimization problem, the manipulated variables are applied to the process to attain the desired economical operation. The following steps have to be carried out at each sampling time of the simulation cycle:

1- Linearizing the simplified model according to Section 7.3.4
2- Estimate the current state of the process x_t
3- Solve the EMPC optimization problem defined by Equations (98)
4- Apply the control setpoint obtained from the EMPC to the temperature controllers
5- Simulate the process model for one sampling time

9 Simulation Results

This chapter presents the simulation results of the implemented models, described in Section 7.3. The simplified and linearized model for the MHF are compared to the mechanistic model quantitatively. The quantification reference for this comparison is the coefficient of determination, denoted as R^2. This coefficient permits a simple way to discern if the simplified and linear models are a valid representation of the process described by the mechanistic model.

A series of tests were designed for the purpose of analyzing the dynamic response of the different models, and to finally make a comparison. The tests include a series of step changes to input variables at different times. The variables used in these tests are: the kaolin feed, total gas flow ratio to the feed, and the ratio of hearth 4 gas flow to the total gas flow, constrained according to the following:

$$F_K \in [26, 40]\ Kg/rotation$$

$$F_g/F_K \in [3.06,3.18]\ mol/Kg$$

$$F_{g4}/F_g \in [0.59, 0.65]$$

The reason to introduce the abovementioned constraints is to ensure that the considered input signals agree within the commonly used process conditions. In the following figure the input series considered in this comparison is presented:

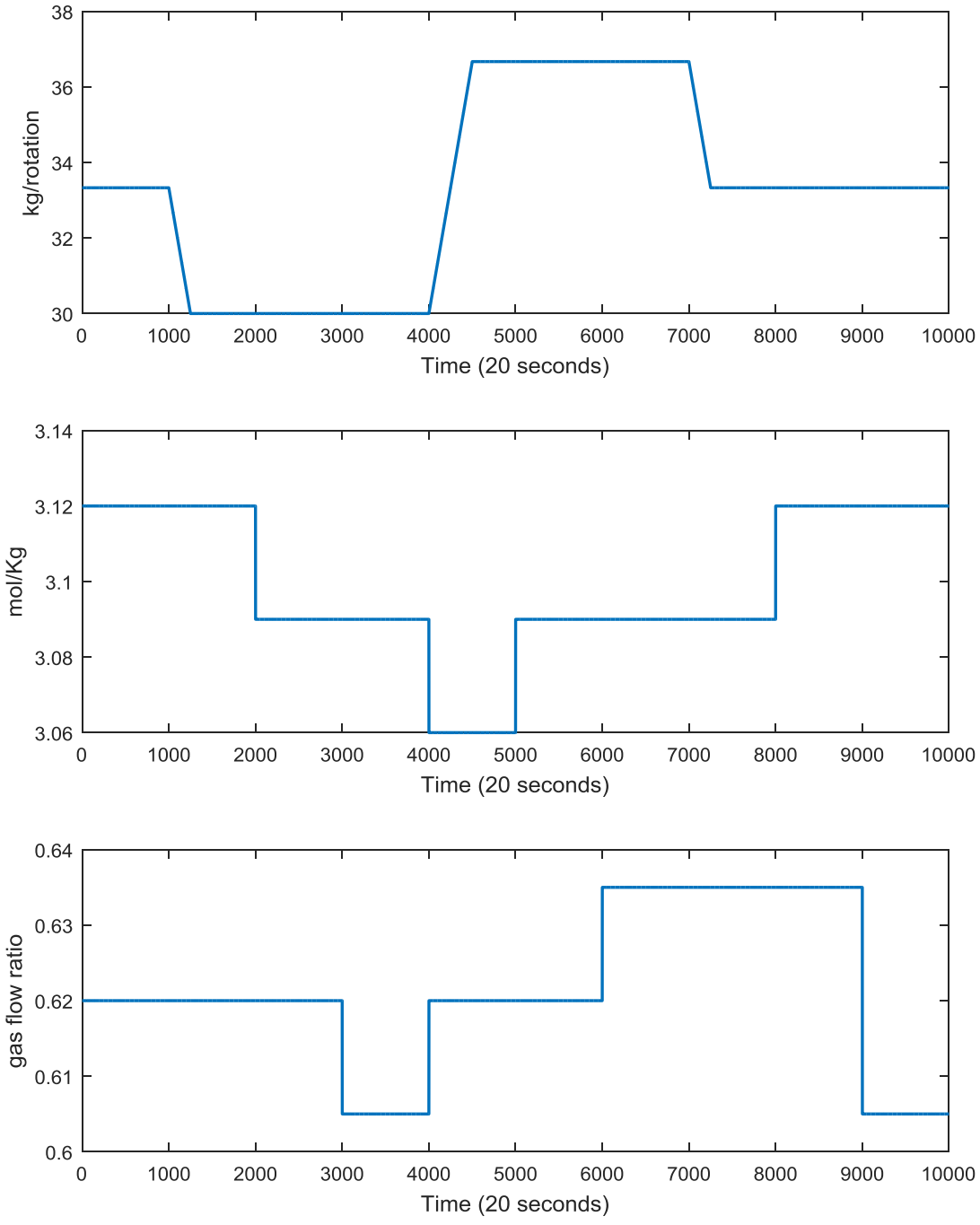

Figure 19. series of inputs changes for response analysis in the different models, F_K (top), F_g/F_K (middle), F_{g4}/F_g (bottom)

In *Figure 19*, the sampling time is based on the shaft rotations periods instead of seconds or minutes, according to how it was used by the mechanistic model in [37]. In the top graph are observed the ramp changes of the kaolin feed to be introduced into the process. First, the kaolin feed is reduced from 33.33 to 30 Kg/rotation after sample 1000. The feed maintains the same value until time 4000, were a new ramp increase occurs from 30 to 36.67 Kg/rotation. The feed is maintained constant at 36.67 Kg/rotation until sample 7000, were the final ramp decrease occurs, from 36.67 to 33.33 Kg/rotation. The latter value is maintained constant for the remaining of the simulation ending at sample 10000.

The second series for the testing is illustrated in the middle graph from the previous figure. The final series of step changes is visualized in the bottom chart of *Figure 19*. The changes are performed to the F_{g4}/F_g ratio. For these tests a number of step changes are performed.

In the following figures, the simulated outputs are given for each of the models. The results include the important sections of the furnace, these are: Heart 1, Heart 4 and Hearth 7.

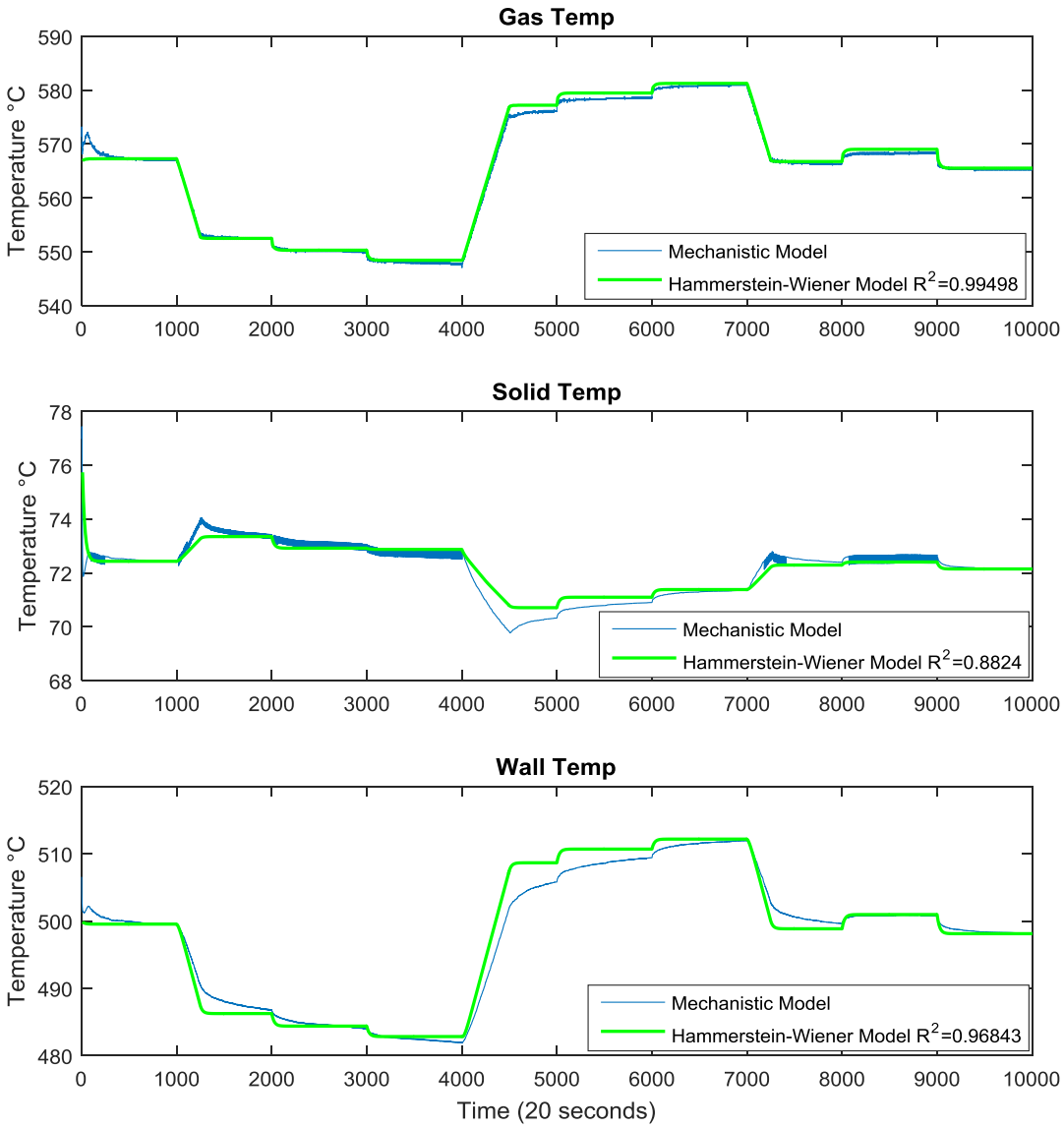

Figure 20. Comparison between model responses in Hearth 1

The importance of presenting the Hearth 1 comes from the fact that in this region of the furnace is where the solid phase is introduced to the process, subsequently begins to dehumidify and rise its temperature, through heat exchange with the gas phase. The figure above presents the simulation results for gas, solid and wall temperatures in Hearth 1, given the series of changes of the input variables, presented earlier in this Chapter. These changes are applied to the upgraded mechanistic model with the wall model, and the simplified model, described in Section 7.3.

The top of *Figure 20* provides the gas phase temperature of Hearth 1 after introducing the series of changes in the input variables. It is noticeable that every 1000 time samples a response change occurs, this will persist throughout the furnace temperature values for each Hearth. Initially it is observed that the simplified model follows remarkably close the response of the mechanistic model. The comparison between the two models is achieved using the coefficient of determination R^2. The simplified model R^2 has a value of 0.99498 for the gas temperature, similarly for the solid and wall temperatures the R^2 is 0,8824 and 0,96843 respectively. This means that the simplified model gives a remarkable prediction for all temperatures. The reason for this is that the simplified model includes the nonlinearities associated with the process, therefore can explain the behavior of the MHF in a proper manner.

Next the simulations of Hearth 4 are presented. In Hearth 4 the Metakaolin is formed and in this location the solid begins its transformation to the spinel phase, which is later reinforced in Hearth 6, as described in Section 6.1.

Figure 21 depicts the response based on the sequence of the input variables, in Hearth 4. At first glance it is noticeable that the behavior of the simplified model, for the gas temperature, follows outstandingly close the response from the mechanistic model, with a R^2 value of 0.9526. The solid temperature follows closely the response from the mechanistic model with a R^2 value of 0.80735. In the case of the wall temperature, the simplified model performs with reduced accuracy compared to other cases, the reason for this could be the limitation on the simplified model to predict the exothermic reaction that begins to occur in the hearth 4. This reaction is difficult to predict, and thus creates overshoots in the temperature, these overshoots are also observable in the solid temperature chart, near time samples 1000, 4000 and 7000.

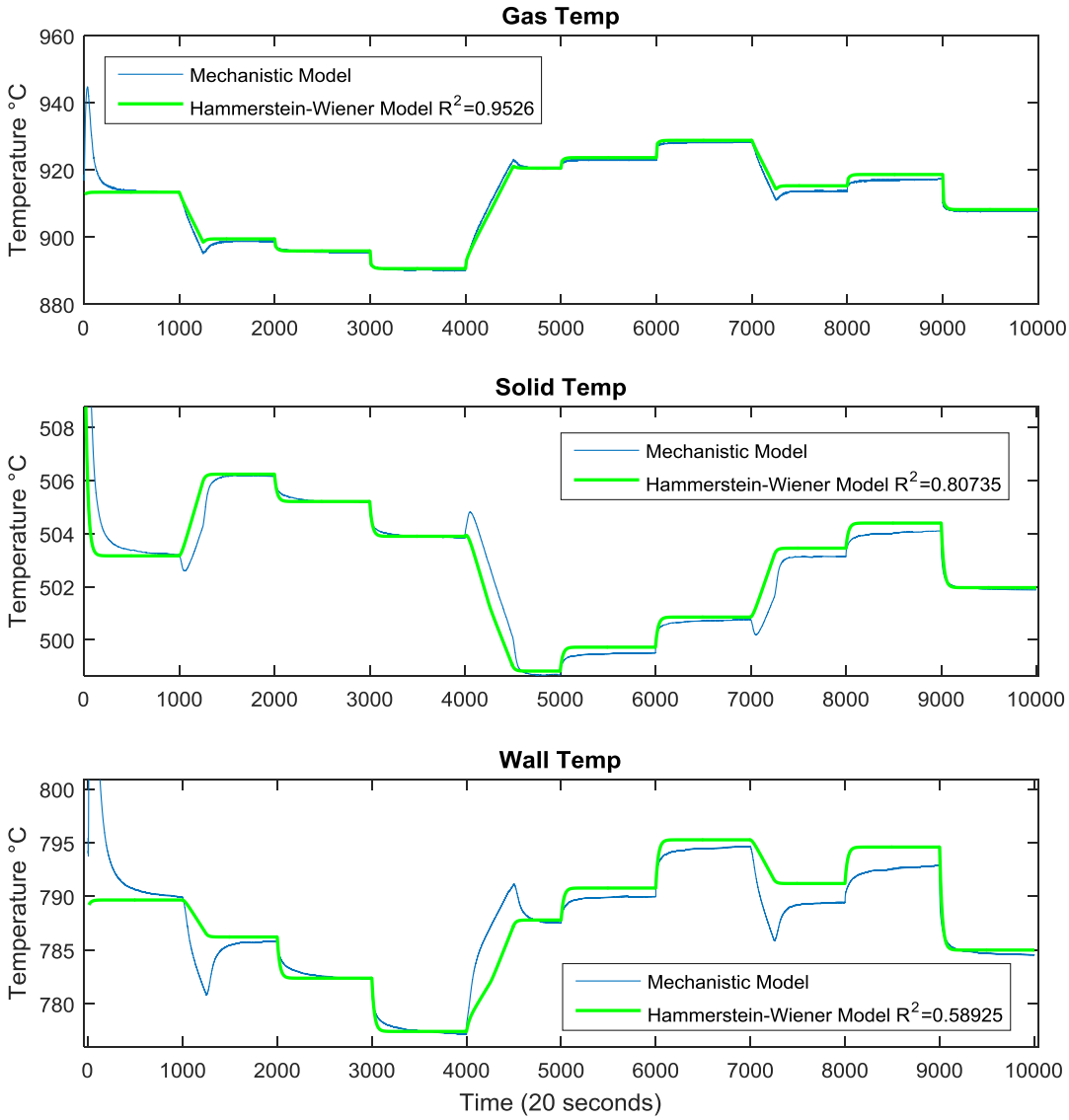

Figure 21. Comparison between the model responses in the Hearth 4

The final section of the Herreschoff calciner analyzed is Hearth 7. In this Hearth the spinel phase begins its cooling down before leaving the process after the Hearth 8.

A comparison between the models presented is accomplished for Hearth 7. In *Figure 22* the different temperatures of Hearth 7 are estimated and compared. Initially it is noticeable how the simplified model describes accurately the expected behavior from the mechanistic model.

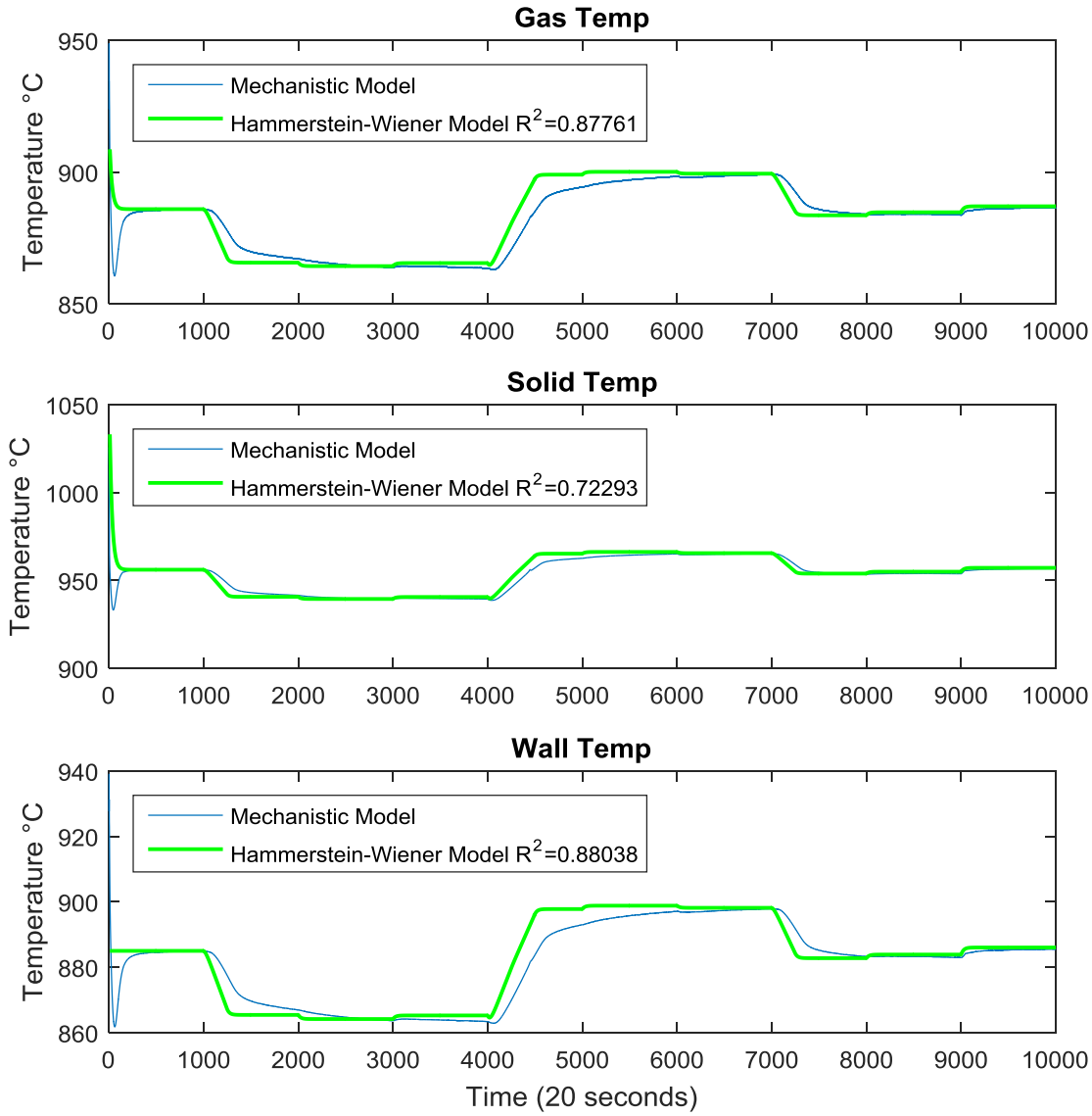

Figure 22. Comparison between model responses in the Hearth 7

To conclude, the results provided by the simplified model are always accurate. Thus, the simplified model may be regularly linearized during the closed loop EMPC simulations in order to maintain the good accuracy of the model used by the MPC implementation.

10 Practical perspectives on EMPC implementation

10.1 Burner Configuration in the Hearth 4

Many process equipment face operation difficulties after design, this might create a scenario of unexpected behavior during process control. The reason for this behavior could possibly be, due to a change in production levels, sizing, or operation outside the intended design performance. In the case of furnaces an important phenomena that occurs is a flame interaction. This phenomena is characterized by the creation of a dense fire cloud, alteration of the heat flux distribution inside the furnace, a rise in NO_x emissions, among others [49].

Over the years there has been an interest from industry, to reduce the NO_x emissions in multi burner furnaces, therefore new burner technologies has been introduced to address this demand. Generally these technologies use a type of furnace gas recirculation in order to reduce the flame temperature, subsequently reducing the formation of NO_x emissions. However, to lower the flame temperature, a reduction in the concentration of air is needed, this brings as a consequence that the flames to be much longer. When the flames, in the modern multi burner furnaces, have increased length and volumetric heat release density, then this situation might lead to a phenomenon known as burner-to-burner (BtoB) interaction [50].

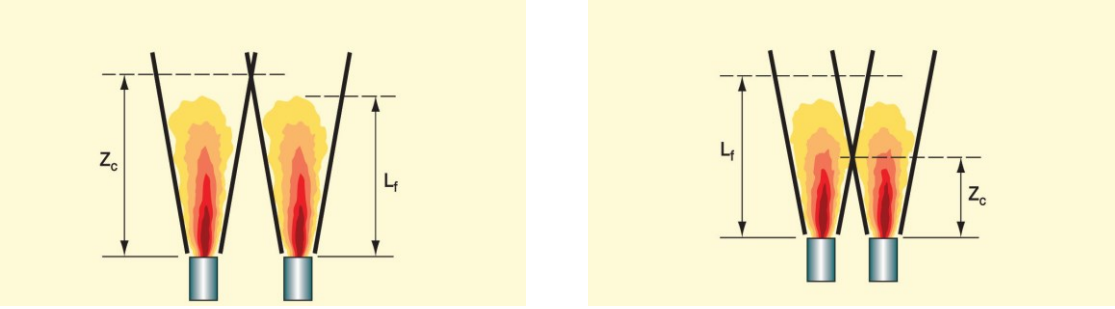

Figure 23. Condition of interaction between two adjacent diffusion flames. Lf < Zc (no flame interaction); Lf > Zc (flame interaction) [35]

Take in Consideration two diffusion flames, as shown in Figure 23 that are neighboring to each other. The flame height is defined here as Lf. Also there is a

critical height where the jets interact (Zc). If the flame height is less than the critical height (Lf < Zc), no BtoB interaction will occur. If the flame height is larger than the critical height (Lf > Zc), the flames will interact. BtoB [50].

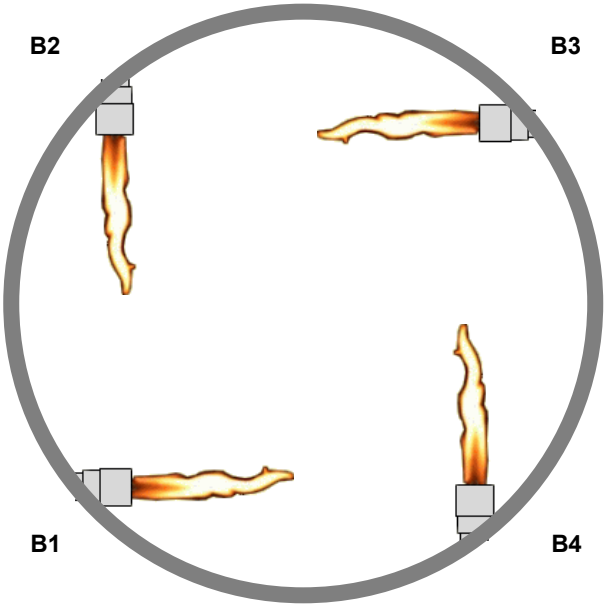

Figure 24. Burners configuration in the multiple hearth furnace

The configuration of the burners inside the furnace gives a clear idea of the interactions that occur inside the furnace. In the figure above (*Figure 24*) it is showed the burner configuration. This configuration is disposed in four equidistant points around the circumference of the hearth. Every burner is located in one of the points and they are facing a contiguous burner as represented in the figure above. Burner 1 (B1) faces burner 4 (B4), B4 faces Burner 3 (B3) and so on.

it is probable that increased capacity operation may give rise to difficulties to control temperature in the Multiple Hearth Furnace. These difficulties are most likely related to the BtoB phenomenon, causing some instabilities and nonlinearities in the temperature control in the Hearth 4. The interaction between the burners may cause a nonlinear correlation between gas flow and temperature in hearth 4. The scenario of burner interactions might be the reason for the rise of nonlinearities during temperature control of a furnace.

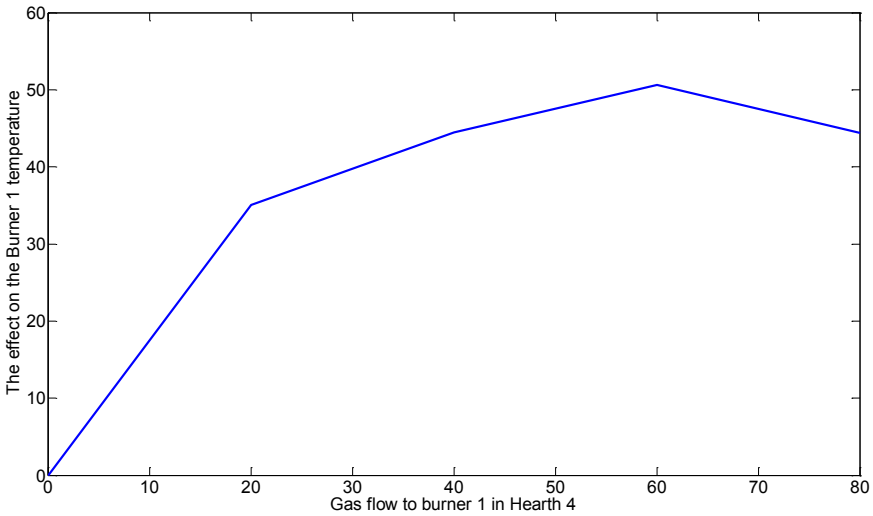

Figure 25. Relationship between the temperature and the gas flow in H4 of the Herreschoff calciner.

From Figure 25 it is noticeable for B1, that after an increase of gas flow over 60 m^3/h the effect on temperature is negative, this means that a rise of gas flow after this point will cause a decrease in temperature. It is important to emphasize that this effect is similar for the other burners, therefore this phenomena is treated in the same manner for the four burners in hearth 4.

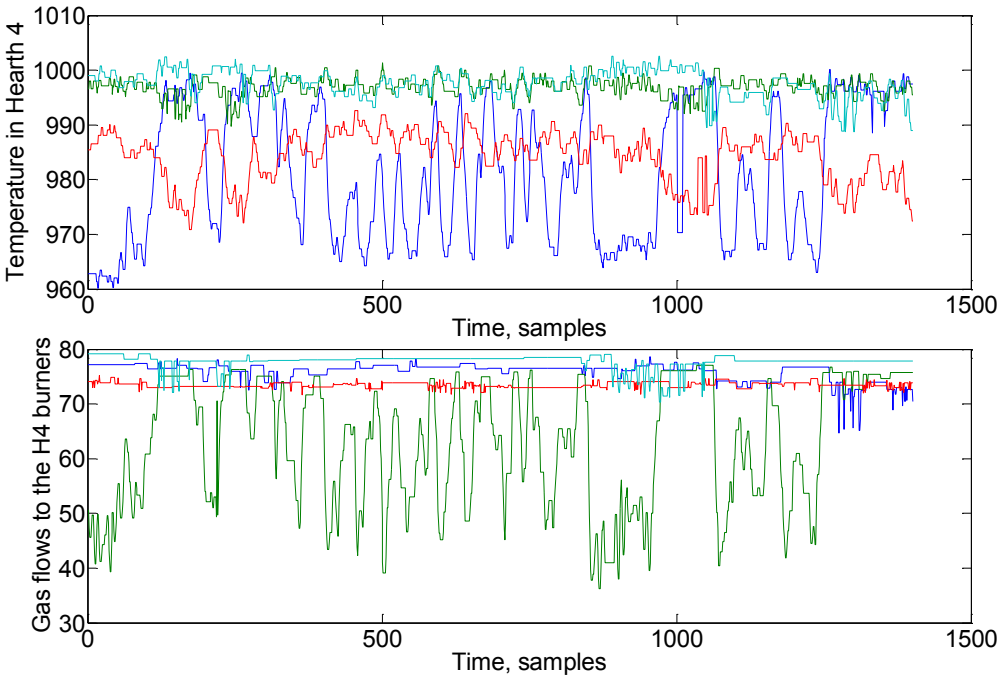

Figure 26. Effect of gas flow on subsequent temperature measurements

The result of the BtoB interaction and the nonlinear effect is confirmed in *Figure 26*. This figure shows process data of the furnace. The top graph shows the temperature of every burner, each associated with a color B1 in blue, B2 in green, B3 in red and finally B4 in light blue. The bottom image displays the gas flow of the burners, using the same color relations. At first glance, it is perceptible the relation between temperature of B1 and gas flow of B2. This relation is direct, indicating that an increase of gas flow in B2 causes an increase of temperature in B1, this occurs most probably due to the burner configuration and the fact that B2 faces directly to B1. A second observation provides that there is a small effect on temperature of B2, even when gas flow of B2 is fluctuating. After observing closely, the gas flow in B2 shown in green has an approximate average of 60 m^3/h. This small change on temperature in B2 is attributed to the nonlinear effect exposed in Figure 25. If gas flow is close to 60 m^3/h the temperature has a small change.

10.2 Simulation studies on temperature control of the Hearth 4

10.2.1 Classical PI controllers

The current control employed in H4 is constituted of 4 PI controllers, one for each burner, and the controllers operate individually. The control scheme is shown in Figure 27.

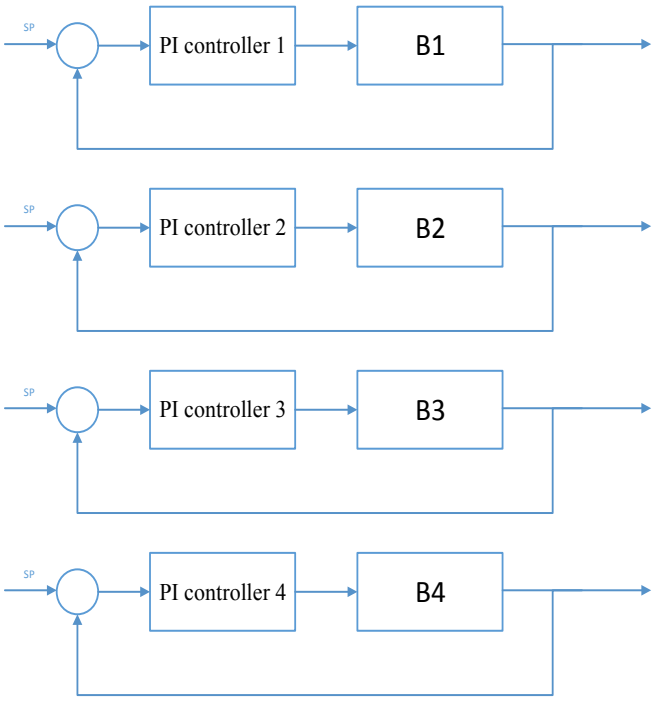

Figure 27. Existing control in Hearth 4

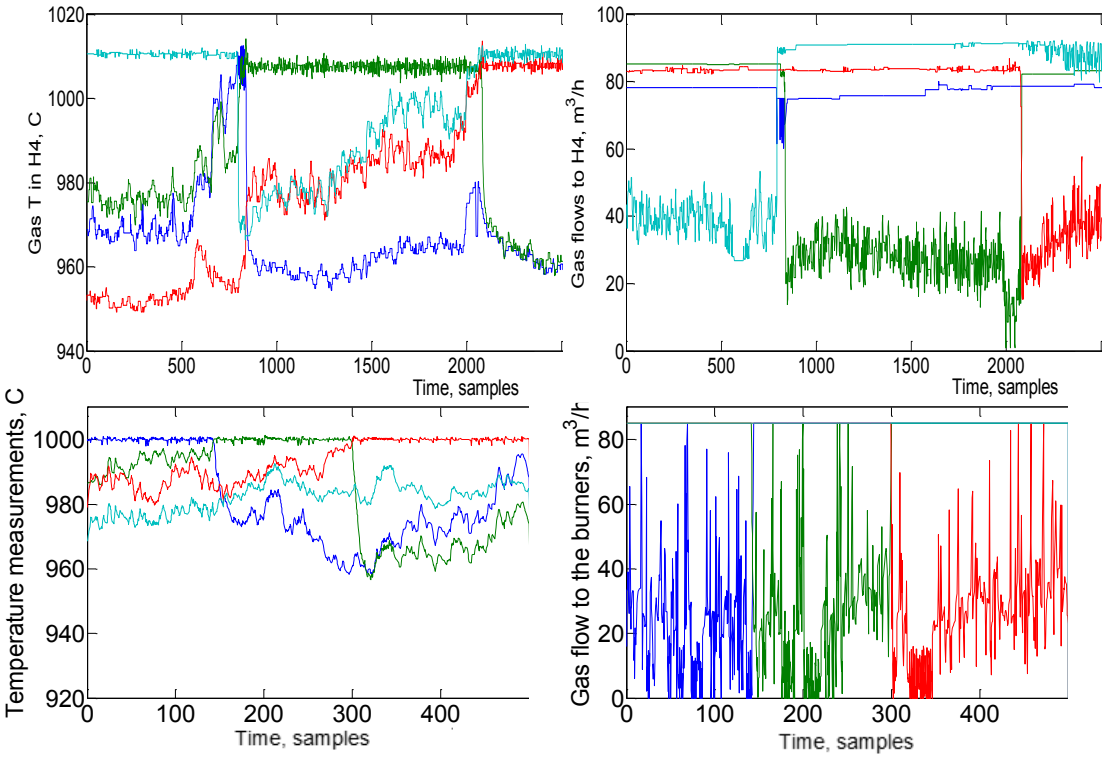

Figure 28. Real process data of H4 (top).
Simulation on current control in H4 (Bottom)

Simulations were made for the purpose of performing tests on the process, and then design a solution for the situation. In the top of *Figure 28* real data of the process is depicted, demonstrating the behavior of H4. In general one burner temperature, at a given time, follows the setpoint. This is illustrated in the top left graph. In the top right figure the gas flows for the burners are shown. In this case only one gas flow is manipulated while the rest remain in saturation. All behavior of the process is the result of the phenomena explained in section 10.1. In the bottom of the figure, the results of the current control are shown as a simulation. The setpoint is fixed to 1000 °C for all burners. The behavior of the simulated process closely resembles the real process, with only one temperature following the setpoint and the gas flows not associated to the stable temperature are in a state of saturation, as shown in the bottom right. For the purpose of this work the

simulations presented follow the main behavior of nonlinearity and interaction, and are used as a basis to develop a solution.

A series of simulations were made in order to show the behavior of the system for 2 operation energy levels. These simulations include two setpoints, the first one being 1000 °C, is considered a high energy operation. The high energy operation uses values of gas flow from 60-85 m^3/h, this range as shown previously in Figure 25, has an inverse proportionality to temperature, and therefore it is more difficult to control. The second setpoint is 960 °C, this value is considered a low energy operation, with gas flow ranging from 0 to 60 m^3/h.

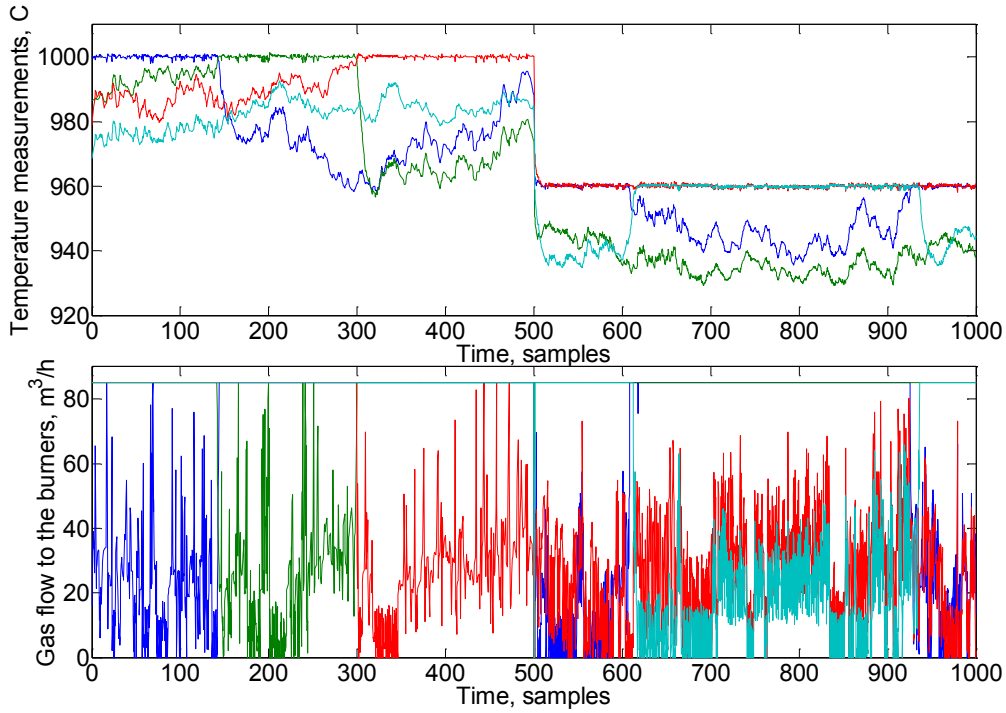

Figure 29. Simulation of change of setpoint, on current control scheme for H4

As portrayed in *Figure 29* the first 500 time samples follow a setpoint of 1000 °C with corresponding manipulated gas flows. Time samples from 501-1000 follow a setpoint of 960 °C also with corresponding manipulated variables. For the first part (1000 °C setpoint) the temperature is only achieved by a burner at a time,

one control loop working, switching after a certain period, while others are in an uncontrolled state. Two burner temperatures follow the desire state in the case for setpoint of 960 °C, with two control loops not working properly, equally changing after a certain time.

10.2.2 Mean temperature control

A proposed solution for the current situation in H4, is the design of a controller that operates on the average temperature of the burners, instead of controlling each burner individually. There is the possibility that in high energy operation the temperature of 1000 °C is not achievable by the system.

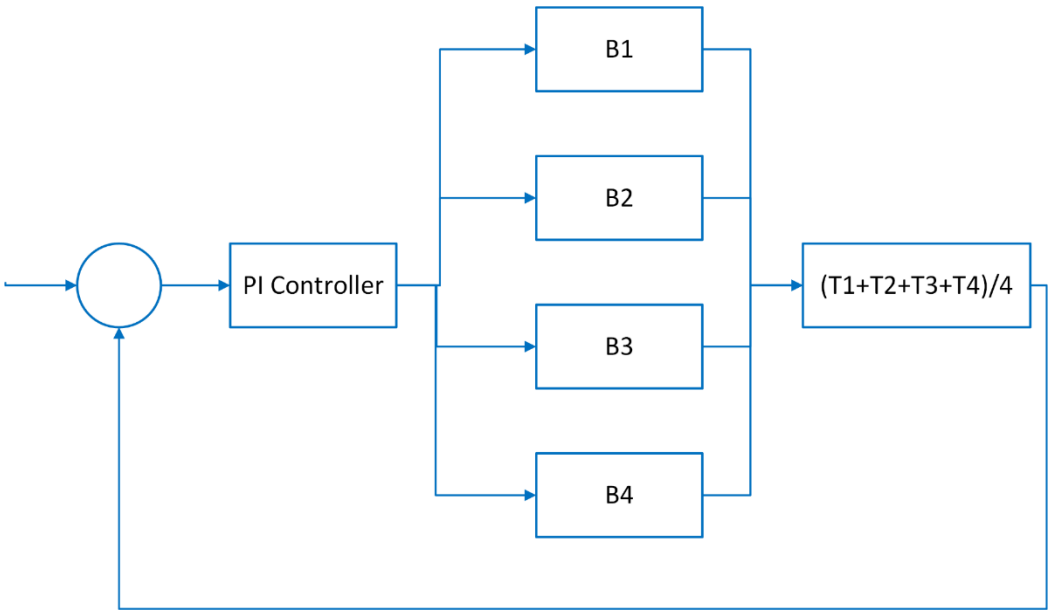

Figure 30. Mean temperature control for H4

The schematic of the mean temperature control is displayed in *Figure 30*. The controller consists of the detection of temperature of the four burners and the calculation of the average value. Based on this calculation control measures are applied to the system by the manipulation of gas flows. Every gas flow is manipulated by the exact same amount.

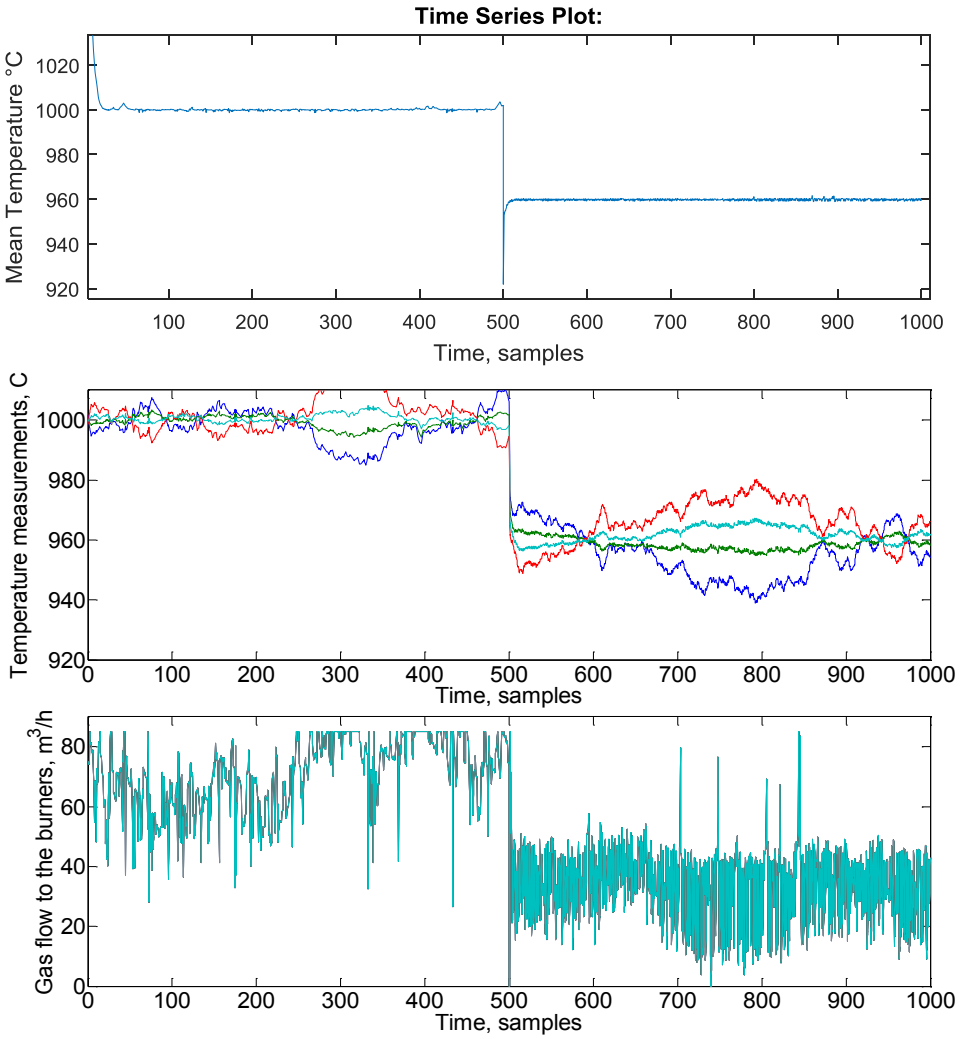

Figure 31. Simulation of change of setpoint, on mean control scheme for H4

After implementation a simulation of the mean control is obtained and shown in *Figure 31*. It is evident that the controller follows the setpoint very closely in both energy operations, as presented in the top graph. The mean temperature on the first 500 time samples is near 1000 °C, while for the second half the mean temperature is fixed to 960 °C. The middle picture illustrates the evolution of temperatures of all burners throughout the simulation. Finally the bottom figure shows how each gas flow is manipulated to achieve the desired control.

10.2.3 Switching Control

A different approach to solve the problem would be to consider the causes of the current behavior as explained before in Section 10.1. So based on the interactions and nonlinearity a control scheme has been devised as switching control. The function of the controller is very simple. It consider two energy operations, low and high energy.

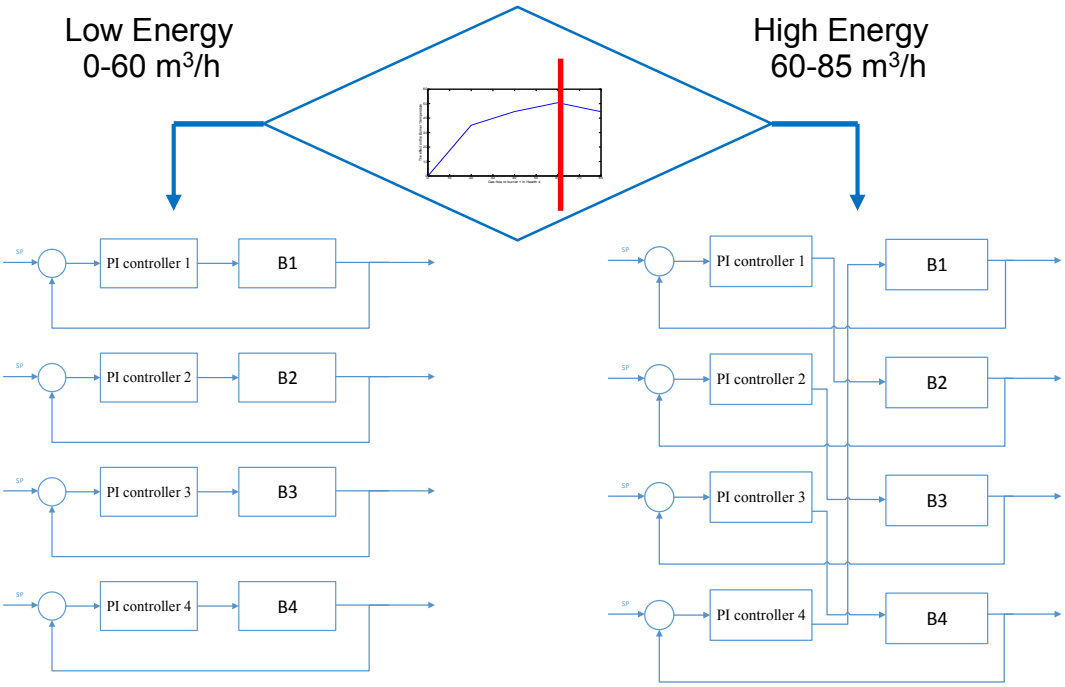

Figure 32. Switching control for H4

The low energy operation stablishes the control as it is currently implemented with a limit of 60 m^3/h, while the high energy control is reconfigured to control temperature in one point with the influencing burner, manipulating gas flows from 60 to 85 m^3/h. In other words, since for example B2 interacts with B1 then the control is rewired to control temperature in B1 by manipulating gas flow in B2, and so subsequently. The controller detects an energy operation from the fixation of gas flows at 60 m^3/h for a few time samples. For example, starting with a setpoint of 1000 °C, the control uses the high energy configuration with the scheme shown on the right side of *Figure 32*. After a change to 960 °C the gas flows start to

decrease until they reach a mean of 60 m^3/h, if every gas flows maintains this level for 5 time samples, then the controller switches to the low energy configuration. In the same manner occurs a change from the low energy to the high energy configuration, after gas flows saturate at 60 m^3/h during 5 time samples.

Once the implementation was completed a simulation of the response was obtained. As portrayed in the top of *Figure 33*, the temperature of all burner follow the setpoint remarkably close for the first and second half of the simulation. It is visible the period for the switching of controllers; this occurs five time samples

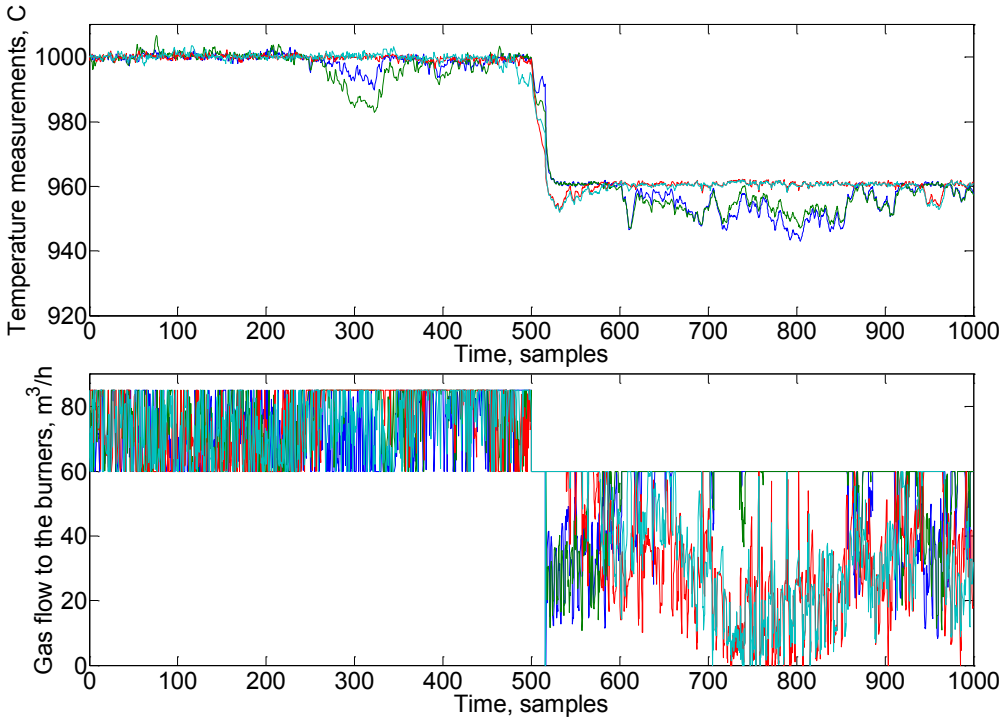

Figure 33. Simulation of change of setpoint, on switching control scheme for H4 after the 500 samples mark, in the bottom of the figure.

11 Conclusions

This thesis focused on the design of a simulation testing environment for advanced control strategies (EMPC, MPC) on the Multiple Hearth Furnace aiming to improve the energy efficiency of the process while maintaining the specified product quality. In the literature part, the fundamentals of Model Predictive Control were presented, including the underlying concepts of Economic MPC. The kaolin processing was described briefly, and the calcination furnace was introduced. A review of control methods used in industry for the control of similar calcination furnaces was presented.

The design of the simulation environment was developed in the experimental part based on several components: a mechanistic model developed previously, an improved wall model, a simplification of the mechanistic model, a linearization method to facilitate implementation in EMPC.

In contrast to the mechanistic model, including hundreds of various equations, the simplified model is implemented in the form of Hammerstein-Wiener nonlinear dynamic model with a reduced number dynamic equations, thus, making MPC implementation possible. Furthermore, the EMPC optimization problem has been formulated mathematically.

Next, a procedure for the linearization of the simplified model, that is necessary for the MPC implementation, was developed. The mechanistic model, and simplified model were tested. The comparison showed that the simplified model follows accurately the mechanistic model in all cases. Thus, a linear model is unable to represent the furnace dynamics properly, and the linearization of the simplified model should be made at each MPC sampling time for obtaining accurate model predictions.

As the EMPC is designed to provide setpoints to basic controllers tracking the temperature in Hearths 4 and 6, the accuracy of the temperature setpoints tracking is essential for the overall control performance. Thus, some suggestions were provided in the thesis for the control in Hearth 4, including a mean temperature control and a switching control. Based on the simulation results, it was concluded that the proposed controller were able to track the temperature setpoints sufficiently well.

12 References

[1] B. A. Ogunnaike and W. H. Ray, Process dynamics, modelling, and control, 1st ed., New York, USA: Oxford University Press, 1994.

[2] J. B. Rawlings, "Tutorial: Model Predictive Control Technology," in *American Control Conference*, San Diego, California, USA, 1999.

[3] J. B. Rawlings, D. Angeli and C. N. Bates, "Fundamentals of Economic model predictive control," in *Conference on Decision and Control*, Maui, Hawai, Usa, 2012.

[4] M. Ellis, H. Durand and P. D. Christofides, "A tutorial review of economic model predictive control methods," *Journal of Process Control,* vol. 24, no. 8, p. 1156–1178, 2014.

[5] J. B. Jørgensen and L. N. Petersen, "Real-time economic optimization for a fermentation process using Model Predictive Control," Strasbourg, France, 2014..

[6] L. T. Biegler and A. Gopalakrishnan, "Economic Nonlinear Model Predictive Control for periodic optimal operation of gas pipeline networks," *Computers & Chemical Engineering,* vol. 52, p. 90–99, 2013.

[7] S. Liu, J. Zhang and J. Liu, "Economic MPC with terminal cost and application to an oilsand primary separation vessel," *Chemical Engineering Science,* vol. 136, p. 27–37, 2015.

[8] J. B. Jørgensen, R. Halvgaard, N. K. Poulsen and H. Madsen, "Economic Model Predictive Control for Building Climate Control in a Smart Grid," Washington, DC, USA, 2012.

[9] P. D. Christofides, X. Chen, M. Heidarinejad and J. Liu, "Distributed economic MPC: Application to a nonlinear chemical process network," *Journal of Process Control,* vol. 22, no. 4, p. 689–699, 2012.

[10] I. K. Craig and L. E. Olivier, "Model-plant mismatch detection and model update for a run-of-mine ore milling circuit under model predictive control," *Journal of Process Control,* vol. 23, no. 2, p. 100–107, 2013.

[11] J. B. Rawlings and D. Q. Mayne., Model Predictive Control: Theory and Design., 1st ed., Madison, WI,: Nob Hill Publishing, 2009.

[12] E. F. Camacho and C. Bordons Alba, Model Predictive Control, 1st ed., Springer, 1999.

[13] B. Huang and R. Kadali, Dynamic Modeling, Predictive Control and Performance Monitoring: A Data-driven Subspace Approach, Springer Science & Business Media, 2008.

[14] E. F. Camacho and C. Bordons, Model Predictive Control in the Process Industry, Advances in Industrial Control, Springer Science & Business Media, 2012.

[15] J. Rossiter, Model-Based Predictive Control: A Practical Approach, CRC Press, 2003.

[16] D. A. Carlson, A. B. Haurie and A. Leizarowitz, Infinite Horizon Optimal Control, Springer Verlag, 1991.

[17] C. E. García, D. M. Prett and M. Morari, "Model Predictive Control: Theory and Practice-a Survey," *Automatica,* vol. 25, no. 3, p. 335–348, 1989.

[18] J. Richalet, Practique de la commande predictive, Hermes, 1992.

[19] D. Clarke and C. Mohtadi, "Properties of generalized predictive control," *Automatica,* vol. 25, no. 6, pp. 859-875, 1989.

[20] M. Ellis and P. D. Christofides, "Unifying Dynamic Economic Optimization and Model Predictive Control for Optimal Process Operation," in *2013 American Control Conference (ACC)*, Washington, DC, USA, 2013.

[21] T. Backx, O. Bosgra and W. Marquardt, "Integration of model predictive control and optimization of processes," in *IFAC symposium on advanced control of chemical processes*, Pisa, Italy, 2000.

[22] J. B. Rawlings, D. Bonné, J. B. Jørgensen, A. N. Venkat and S. B. Jørgensen, "Unreachable setpoints in model predictive control," *IEEE Transactions on Automatic Control,* vol. 53, no. 9, pp. 2209-2215, 2008.

[23] J. B. Rawlings and R. Amrit, "Optimizing process economic performance using model predictive control.," in *Nonlinear Model Predictive Control - Towards New Challenging Applications*, Springer, 2009, p. 119–138.

[24] J. B. Rawlings, D. Angeli and R. Amrit, "On Average Performance and Stability of Economic Model Predictive Control," *IEEE Transactions on Automatic Control,* vol. 57, no. 7, p. 1615–1626, 2012.

[25] P. D. Christofides, M. Heidarinejad and J. Liu, "State-estimation-based economic model predictive control of nonlinear systems," *Systems & Control Letters,* vol. 61, no. 9, p. 926–935, 2012.

[26] M. Ellis and P. D. Christofides, "Economic Model Predictive Control with Time-Varying Objective Function for Nonlinear Process Systems," *AIChE Journal,* vol. 60, no. 2, pp. 507-519, 2014.

[27] D. Angeli, R. Amrit and J. B. Rawlings, "Enforcing Convergence in Nonlinear Economic MPC," in *50th IEEE Conference on Decision and Control and European Control Conference*, Orlando, FL, USA, 2011.

[28] R. Amrit, J. B. Rawlings and L. T. Biegler, "Optimizing process economics online using model predictive control," *Computers and Chemical Engineering,* vol. 58, p. 334– 343, 2013.

[29] J. B. Rawlings, M. Diehl and R. Amrit, "A Lyapunov Function for Economic Optimizing Model Predictive Control," *IEEE TRANSACTIONS ON AUTOMATIC CONTROL,* vol. 56, no. 3, pp. 703-707, 2011.

[30] C. Thurlow, China Clay from Cornwall and Devon: An Illustrated Account of the Modern China Clay Industry, 4th ed., St Austell: Cornish Hillside Publications, 2005.

[31] H. H. Murray, Applied clay mineralogy - Occurrences, Processing and Application of Kaolins, Bentonites, Palyqorskite-Sepiolite, and Common Clays, Indiana University, Bloomington, USA: Elsevier, 2006.

[32] H. H. Murray and J. E. Kogel, "Engineered clay products for the paper industry," *Applied Clay Science,* vol. 29, no. 3-4, p. 199– 206, 2005.

[33] H. H. Murray, "Clays," in *Ullmann's encyclopedia of industrial chemistry.*, Indiana, United States, Wiley-VCH, 2006.

[34] P. Ptáček, D. Kubátová, J. Havlica, J. Brandštetr, F. Šoukal and T. Opravil, "Isothermal kinetic analysis of the thermal decomposition of kaolinite: The thermogravimetric study," *Thermochmica Acta,* vol. 501, no. 1-2, pp. 24-29, 2010..

[35] P. Ptáček, D. Kubátová, J. Havlica, J. Brandštetr, F. Šoukal and T. Opravila, "The non-isothermal kinetic analysis of the thermal decomposition of kaolinite by thermogravimetric analysis," *Powder technology,* vol. 204, no. 2-3, p. 222–227, 2010.

[36] P. Ptáček, T. Opravil, F. Šoukal, J. Wasserbauer, J. Másilko and J. Baráček, "The influence of structure order on the kinetics of dehydroxylation of kaolinite," *Journal of the European Ceramic Society,* vol. 33, no. 13-14, p. 2793–2799, 2013.

[37] A. Eskelinen, Dynamic Modelling of a multiple hearth furnace, Espoo, Finland: Aalto University, 2014.

[38] P. Ptáček, F. Šoukal, T. Opravil, M. Nosková, J. Havlica and J. Brandštetr, "The kinetics of Al–Si spinel phase crystallization from calcined kaolin," *Journal of Solid State Chemistry,* vol. 183, no. 11, p. 2565–2569, 2010.

[39] R. C. T. Slade, T. W. Davies and H. Atakul, "Flash Calcination of Kaolinite: Mechanistic Information from Thermogravimetry," *Journal of Material Chemistry,* vol. 1, no. 5, pp. 751-756, 1991.

[40] P. Ptáček, F. Šoukal, T. Opravil, J. Havlica and J. Brandštetr, "The kinetic analysis of the thermal decomposition of kaolinite by DTG technique," *Powder Technology,* vol. 208, no. 1, p. 20–25, 2011.

[41] M. Ramírez, R. Haber, V. Peña and I. Rodríguez, "Fuzzy control of a multiple hearth furnace," *Computers in Industry,* vol. 54, no. 1, p. 105–113, 2004.

[42] B. Voglauer and H. Jörgl, “Dynamic Model of a Roast Process for Simulation and Control,” *Mathematical and Computer Modelling of Dynamical Systems,* vol. 10, no. 3-4, pp. 217-230, 2004.

[43] W. Geyrhofer, B. Voglauer and H. P. Jörgl, “Control of a roasting process for the recovery of vanadium,” in *Conference of Control Applications*, Istanbul, Turkey, 2003.

[44] B. Voglauer, W. Geyrhofer and H. P. Jörgl, “A model based control concept with knowledge based overhead control of a roasting process,” in *IEEE American Control Conference*, Boston, Massachusetts, 2004.

[45] R. Gouveia, D. G. Lewis, A. Restrepo, L. A. Rodrigues and R. Gedraite, “Application of Model-Predictive Control to Multi-Hearth Nickel Reduction Roasters,” in *Automation in Mining, Mineral and Metal Processing*, Chile, 2009.

[46] A. Eskelinen, A. Zakharov, S.-L. Jämsä-Jounela and J. Hearle, "Dynamic modeling of a multiple hearth furnace for kaolin calcination," *AIChE Journal,* vol. 61, no. 11, p. 3683–3698, 2015.

[47] J. D. Gilchrist and R. W. Douglas, Fuels, Furnaces and Refractories, Elsevier , 1977 .

[48] Y. Zhu, Multivariable System Identification For Process Control, Elsevier, 2001.

[49] J. Charles E. Baukal, The John Zink Hamworthy Combustion Handbook, Second Edition: Volume 2 – Design and Operations, CRC Press, 2013 .

[50] M. Fleifil, M. Lorra, C. E. Baukal, J. A. Lewallen and D. E. & Wright, "Process burner spacing," *Petroleum Technology Quarterly,* vol. Q, no. 2, pp. 1-5, 2006.